

ON THE MOTION OF A CURVED AND TWISTED SLENDER ROD

ON THE MOTION
OF A
NATURALLY CURVED AND TWISTED SLENDER ROD

By
KENRICK E. PILGRIM, B.Sc.(C.E.)

A Thesis
Submitted to the Faculty of Graduate Studies
in Partial Fulfilment of the Requirements
for the Degree
Master of Engineering

McMaster University

May 1967

MASTER OF ENGINEERING
(Engineering Mechanics)

McMASTER UNIVERSITY
Hamilton, Ontario

TITLE: On the Motion of a Naturally Curved and Twisted
Slender Rod.

AUTHOR: Kenrick E. Pilgrim, B.Sc.(Civil Eng.),
University of Manitoba.

SUPERVISOR: Professor W. K. Tso

NUMBER OF PAGES: x, 76, A21

SCOPE AND CONTENTS:

A set of equations describing the motion of a naturally curved and twisted slender elastic rod is determined in this thesis. In particular, a study of the vibration of a helical spring is made, and the natural frequencies from the theory presented are compared with those from a simpler theory. Comparison of the two theories shows that the simpler theory is valid for most springs. The simpler theory is then used to show how the natural frequencies for a helical spring can be obtained when the spring is subjected to any boundary conditions. Finally, an analytical and experimental study of the vibration of a helical spring clamped at both ends is made in order to investigate the validity of the theory presented.

ACKNOWLEDGEMENTS

The author wishes to express his sincere gratitude for the continuous encouragement and guidance given to him by his Research Supervisor, Dr. W. K. Tso, who suggested the problem. Thanks are also due to Dr. Tso for his kind permission to use a great deal of his work in this thesis, and to McMaster University for the scholarship and teaching assistantship.

The financial support given by the National Research Council of Canada for the research is also acknowledged.

K. Pilgrim

McMaster University,
May, 1967.

CONTENTS

<u>Chapter</u>		<u>Page</u>
I	INTRODUCTION	1
II	FORMULATION OF EQUATIONS OF MOTION	4
	1. Vectorial Formulation of Equations of Motion	4
	2. Simplification of Dynamic Equations	8
	3. Reduction of Equations of Motion	12
	4. Generalised Force-Displacement Relationships	15
	5. Equations of Motion in Terms of Displacement Variables	16
III	DYNAMIC EQUATIONS OF MOTION OF A HELICAL SPRING	19
	1. Introduction	19
	2. Wave Propagation along a Helical Spring	21
	3. Discussion of Spectrum Curves	29
	4. Configuration of the Rod in the Form of a Ring	37
	5. Frequencies for Half Ring Segment	38
	6. Straight Rod Configuration	43
	7. Accuracy of Love's Frequencies	44
IV	GENERAL SOLUTION OF HELICAL SPRING PROBLEM	47
	1. Introduction	47
	2. Nature of Roots of Characteristic Equation	53
	3. Example	54
V	EXPERIMENTAL PROGRAM	60
	1. Introduction	60
	2. Experimental Set Up	63
	3. Equipment	64
	4. Experimental Procedure	66
	5. Experimental Results	68
	6. Discussion of Results	68

<u>Chapter</u>		<u>Page</u>
VI	CONCLUSIONS AND RECOMMENDATIONS	72
	1. Conclusions	72
	2. Recommendations	73
APPENDIX		
	I. Properties of Helical Spring	A1
	II. Half Turn of Spring	A3
	III. Half Turn of Ring	A3
	IV. Example of [D] Matrix Elements - Chapter IV	A4
	V. Derivation of Generalised Force- Displacement Relationships	A6
	VI. Flow Charts and Computer Program	A8
BIBLIOGRAPHY		76

LIST OF FIGURES

<u>Figure</u>		<u>Page</u>
II.1	Rod Segment	5
II.2	Trihedral of Space Curve	7
III.1	Helical Spring	22
III.2a,b	Spring Spectrum Curves - In-plane Frequencies	30-31
III.2c,d	Spring Spectrum Curves - Out-of-plane Frequencies	32-33
V.1	Experimental Set UP	61
V.2	Test Spring in Position	62
V.3	Schematic Diagram of Experimental Set Up	65
A.1	Helical Spring	A1
A.2	Rod Segment	A6
A.3	Wave Propagation Flow Chart	A9
A.4	General Solution Flow Chart	A10
A.5	Computer Program for General Solution	All

LIST OF TABLES

<u>Table</u>		<u>Page</u>
III.1	Theoretical Results - Wave Propagation in Helical Spring	26
III.2	Comparison of Frequencies given by Love and those given without making Love's approximations	46
IV.1	Comparison of Frequencies obtained by the General Solution Method with those obtained from Love's equation	59
V.1	Comparison of Experimental and Theoretical Results - Spring 1	69
V.2	Comparison of Experimental and Theoretical Results - Spring 2	70

LIST OF SYMBOLS

\bar{r}	position vector of a point on axis of curved rod
\bar{R}	position vector relating any point B in a plane perpendicular to the axis of the rod to point ρ where plane cuts axis of rod
R_*	modulus of \bar{R}
\bar{p}	linear momentum vector
ρ	density
\bar{N}_t	axial force vector = $N_t \bar{e}_t$
\bar{N}_o	axial shear force vector origin
\bar{Q}	transverse shear force vector = $Q_1 \bar{e}_1 + Q_2 \bar{e}_2$
\bar{Q}_o	transverse shear force vector at origin
\bar{M}	moment vector = $M_t \bar{e}_t + M_1 \bar{e}_1 + M_2 \bar{e}_2$
\bar{M}_o	moment vector at origin
s	distance measured along axis of rod
t	time
a	radius of gyration of rod for circular sections
l	total length of spring along axis
A	cross-sectional area of rod
ξ	s/a - normalised coordinates measured along axis of rod
\bar{f}	applied load vector

\bar{L}	angular momentum vector
\bar{M}	moment vector = $M_t \bar{e}_t + M_1 \bar{e}_1 + M_2 \bar{e}_2$
\bar{M}_O	moment vector at origin
$\bar{e}_t, \bar{e}_1, \bar{e}_2$	trihedral of space curve - unit vectors in tangential, normal and binormal directions
θ	axial rotation of cross-section of rod
$(\dot{\quad}), (\ddot{\quad})$	$\frac{\partial(\quad)}{\partial t}, \frac{\partial^2(\quad)}{\partial t^2}$ etc.
$(\quad)', (\quad)''$	$\frac{\partial(\quad)}{\partial \xi}, \frac{\partial^2(\quad)}{\partial \xi^2} = D_1, D_2$ etc.
d	rod diameter
r	rod radius
D	spring diameter
R	spring radius
\bar{H}	See equation (II.11)
I	second moment of cross-sectional area
I_p	polar moment of inertia
\bar{r}_O	position vector of axis of rod in unstressed configuration
\bar{u}	displacement vector = $u_t \bar{e}_t + u_1 \bar{e}_1 + u_2 \bar{e}_2$
\bar{U}	normalised displacement vector = $\bar{u}/a = U_t \bar{e}_t + U_1 \bar{e}_1 + U_2 \bar{e}_2$
κ_O, τ_O	curvature and tortuosity of rod
κ, τ	normalised curvature and tortuosity of rod respectively
λ	normalised wavelength = $\pi a/\ell$
α	pitch angle of helical spring
n_t, n_1, n_2, n_θ	constants representing amplitudes of axial, transverse in-plane, transverse out-of-plane and torsional motions

ω	circular frequency
Ω	nondimensional frequency = $\omega a \sqrt{\rho/E}$
N	number of turns of helical spring
μ_i	roots of characteristic equation
E,G	Young's modulus and shear modulus respectively
ν	Poisson's ratio

CHAPTER I
INTRODUCTION

The dynamic behaviour of a rod of circular cross-section, either solid or hollow, the axis of which is in the form of a general space curve is of interest. For example, some members in radar installations are naturally curved and twisted in the form of a space curve. Pipes have been designed to have an axis in the form of a space curve to allow for thermal expansion in chemical plants. Other naturally curved systems of this kind are found in springs, balcony structures and arches. A knowledge of the behaviour of such structural elements subjected to dynamic loads is of value for design purposes.

The static deformation of naturally curved rods is a classical elasticity problem, and many papers have been written on the subject.^{1,2,3,5*} The equations of motion are very complicated when the unstressed state of the rod possesses both curvature and tortuosity.

Previous work on this subject has been done by Love¹. In his study of the stress wave propagation along a helical spring of infinite length, it is assumed that

*Numbers refer to the Bibliography listing.

the torsional inertia of the circular rod is negligible. In addition, he assumed the centerline of the rod to be axially inextensible. Wittrick² also worked on the elastic wave propagation in helical springs, where the wire cross-section is of any doubly symmetrical shape, thus covering rectangular as well as circular sections. In addition, Wittrick took into account shear deformation due to bending. Ojalvo³ studied in detail the vibrations of incomplete rings which can be considered as a very special case of a rod possessing curvature but no tortuosity. Massoud⁴ employed vectorial methods to derive the equations of motion of a naturally curved and twisted rod. However, the result is in vectorial form and is not readily useable. The static deformation of such a rod is also given in Love's treatise on elasticity⁵.

In this study, a simplified set of equations is developed governing the longitudinal, flexural and torsional motions of a circular uniform rod, or thick-walled tube whose natural state is in the form of a space curve. Unlike the previous work which takes into account shear deformation due to bending, the Euler-Bernouilli beam assumption of plane cross-sections remaining plane and perpendicular to the axis both before and after deformation is employed in the present derivation. The rod is assumed to be made of a linearly elastic, isotropic and homogeneous material. The couplings between the various types of motions caused by the initial curvature and tortuosity are

shown explicitly for the case when the rod is in the form of a helix. The equations can be reduced to the dynamic equations of a plane curve, or a straight rod as special cases.

A comparison is made in this thesis on the accuracy of Love's theory by comparing the natural frequencies calculated based on Love's theory and the present theory. A computer program is developed to determine the natural frequencies of a helical rod under different boundary conditions. Finally, a series of tests were performed on two helical springs and the experimental results are compared with the results from theoretical calculations.

CHAPTER II

FORMULATION OF THE EQUATIONS OF MOTION

1. Vectorial Formulation of Equations of Motion

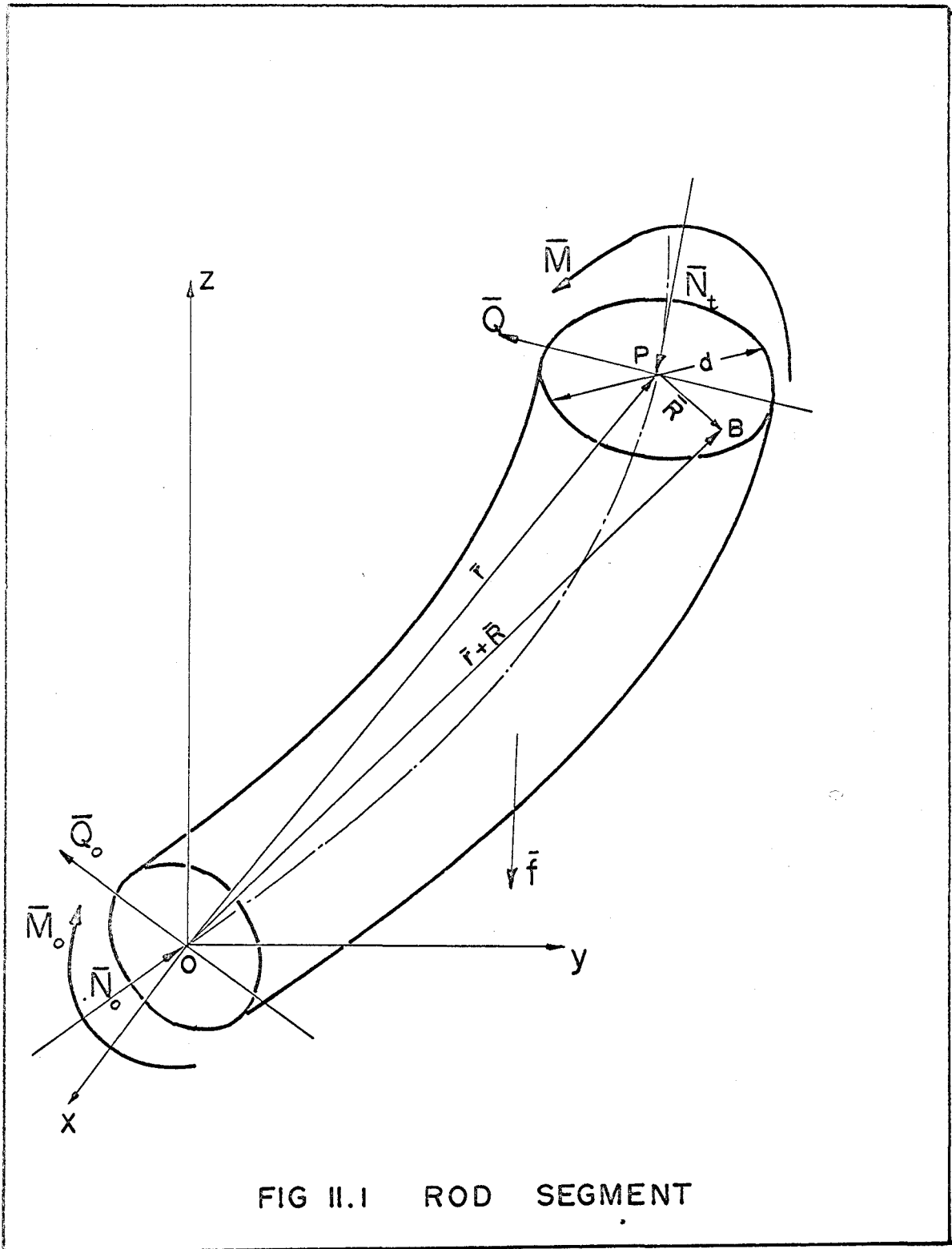
Consider a rod of circular cross-section, either solid or hollow, the axis of which is in the form of a general space curve possessing both curvature and tortuosity. The rod is supported at its ends, and is subjected to loadings distributed along its length. The equations of motion are derived by equating the time rate of change of momentum and moment of momentum to the total forces and moments respectively, acting on a given segment of the rod. The following assumptions are made:

(i) that the cross-sections remain circular after deformation

(ii) that the Euler-Bernouilli assumption holds, i.e., a cross-section of the rod remains plane and perpendicular to the axis of the rod at all times.

Due to such imposed constraints, each section of the rod has four instead of six degrees of freedom, namely three translational displacements and one rotational displacement about the axis of the rod.

Let \bar{r} be the position vector of a point P on the axis of the rod relative to a fixed origin O. \bar{R} is the



position vector relating the position of any point B to P, in a plane perpendicular to the axis of the rod at the point P. The position vector of B is then given by $(\bar{r} + \bar{R})$ as shown in Fig. II.1.

The total linear momentum vector \bar{p} of the rod segment from O to P is

$$\bar{p} = \int_0^{\ell} \int_A \rho \frac{\partial}{\partial t} (\bar{r} + \bar{R}) dA ds \quad \dots (II.1)$$

where s is the distance measured along the axis of the rod, and ℓ is the total distance from O to P measured along the axis, and \int_A denotes integration to be carried out over the cross-sectional area of the rod.

Applying the linear momentum principle yields

$$\frac{d\bar{p}}{dt} = (\bar{N}_t - \bar{N}_0) + (\bar{Q} - \bar{Q}_0) + \int_0^{\ell} \bar{f} ds \quad \dots (II.2)$$

Similarly, the moment of momentum vector \bar{L} for the rod segment is

$$\bar{L} = \int_0^{\ell} \int_A \rho \left[(\bar{r} + \bar{R}) \times \frac{\partial}{\partial t} (\bar{r} + \bar{R}) \right] dA ds \quad \dots (II.3)$$

Applying the moment of momentum principle yields

$$\frac{d\bar{L}}{dt} = \bar{r} \times (\bar{N}_t + \bar{Q}) + (\bar{M} - \bar{M}_0) + \int_0^{\ell} (\bar{r} \times \bar{f}) ds \quad \dots (II.4)$$

Equations (II.2) and (II.4) are now the dynamic equations for the rod subjected to the given loadings.

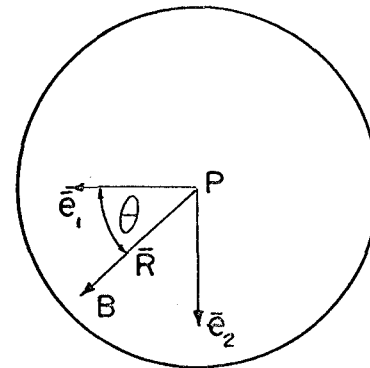
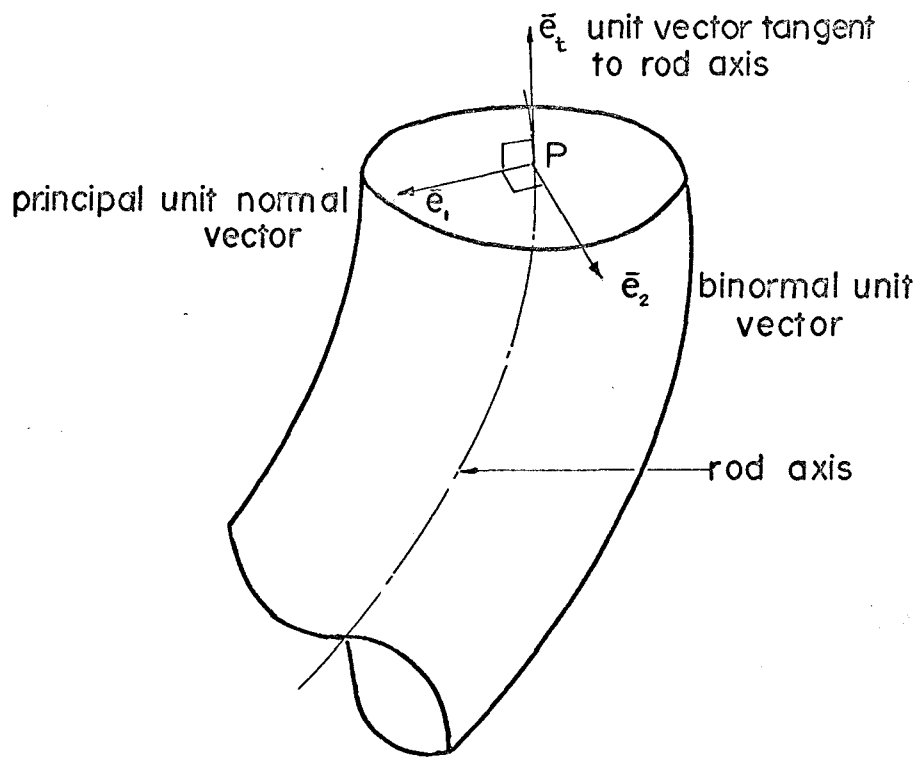


FIG II.2 TRIHEDRAL OF SPACE CURVE

2. Simplification of Dynamic Equations

In order to simplify (II.2) and (II.4), it is convenient to define a set of mutually orthogonal unit vectors \bar{e}_t , \bar{e}_1 and \bar{e}_2 , attached to the point P, where \bar{e}_t is the unit vector tangential to the axis of the rod, \bar{e}_1 is the principal normal and \bar{e}_2 is the binormal at P as shown in Fig. II.2.

The set of unit vectors \bar{e}_t , \bar{e}_1 and \bar{e}_2 is known as the trihedral associated with the space curve. \bar{R} , a vector in the plane of the cross-section can be expressed as

$$\bar{R} = (R_* \cos \theta) \bar{e}_1 + (R_* \sin \theta) \bar{e}_2 \quad \dots(\text{II.5})$$

$$\text{and } \frac{\partial \bar{R}}{\partial t} = R_* \left[\cos \theta \frac{\partial \bar{e}_1}{\partial t} + \sin \theta \frac{\partial \bar{e}_2}{\partial t} + (\cos \theta \bar{e}_2 - \sin \theta \bar{e}_1) \frac{\partial \theta}{\partial t} \right] \quad \dots(\text{II.6})$$

where θ represents the rotation of the section of the rod about its axis. The right hand side of (II.1) can be written as

$$\rho \int_0^l \int_0^R \int_0^{2\pi} R_* \left[\frac{\partial \bar{r}}{\partial t} + \frac{\partial \bar{R}}{\partial t} \right] d\theta dR_* ds,$$

and since

$$\int_0^{2\pi} \frac{\partial \bar{R}}{\partial t} d\theta = 0, \text{ and } \bar{r} \text{ is dependent of } \theta,$$

(II.1) reduces to

$$\bar{p} = \rho A \int_0^l \frac{\partial \bar{r}}{\partial t} ds \quad \dots(\text{II.7})$$

Substituting (II.7) into (II.2) yields

$$\rho A \int_0^{\ell} \ddot{\bar{r}} ds = (\bar{N}_t - \bar{N}_0) + (\bar{Q} - \bar{Q}_0) + \int_0^{\ell} \bar{f} ds$$

$$\text{or } \int_0^{\ell} \left[\rho A \ddot{\bar{r}} - \frac{\partial}{\partial s} (\bar{N}_t + \bar{Q}) - \bar{f} \right] ds = 0 \quad \dots \text{(II.8)}$$

If (II.8) holds for all values of ℓ , it is necessary that the integrand be zero, i.e.,

$$\rho A \ddot{\bar{r}} = \frac{\partial}{\partial s} (\bar{N}_t + \bar{Q}) + \bar{f} \quad \dots \text{(II.9)}$$

Similarly, (II.4) can be simplified. (II.3) can be written

as

$$\bar{L} = \int_0^{\ell} \int_A \rho [\bar{r} \times \dot{\bar{r}} + \bar{R} \times \dot{\bar{R}} + \bar{r} \times \dot{\bar{R}} - \dot{\bar{r}} \times \bar{R}] d\theta R_* dR_* ds.$$

\bar{r} and $\dot{\bar{r}}$ are independent of θ , and \bar{R} and $\dot{\bar{R}}$ are dependent on θ as shown by (II.5) and (II.6). But $\int_0^{2\pi} \sin\theta d\theta = \int_0^{2\pi} \cos\theta d\theta = 0$

$\therefore \int_A (\bar{r} \times \dot{\bar{R}} - \dot{\bar{r}} \times \bar{R}) d\theta = 0$, and (II.3) can be written as

$$\begin{aligned} \bar{L} &= \int_0^{\ell} \int_A \rho [\bar{r} \times \dot{\bar{r}} + \bar{R} \times \dot{\bar{R}}] d\theta R_* dR_* ds \\ &= \rho \int_0^{\ell} A (\bar{r} \times \dot{\bar{r}}) ds + \rho \int_0^{\ell} \int_0^{\frac{d}{2}} \int_0^{2\pi} (\bar{R} \times \dot{\bar{R}}) d\theta R_* dR_* ds \end{aligned}$$

The second term on the right hand side of the above equation can be written after substituting for \bar{R} and $\dot{\bar{R}}$ as

$$\begin{aligned}
& \rho \int_0^l \int_0^{\frac{d}{2}} \int_0^{2\pi} R_*^3 (\cos\theta \bar{e}_1 + \sin\theta \bar{e}_2) \times \left[(\dot{\bar{e}}_1 + \bar{e}_2 \dot{\theta}) \cos\theta + (\dot{\bar{e}}_2 - \bar{e}_1 \dot{\theta}) \sin\theta \right] d\theta dR_* ds \\
&= \rho \int_0^l \int_0^{\frac{d}{2}} \int_0^{2\pi} R_*^3 \left\{ [\bar{e}_1 \times \dot{\bar{e}}_1 + \bar{e}_1 \times \bar{e}_2 \dot{\theta}] \cos^2\theta + [\bar{e}_2 \times \dot{\bar{e}}_2 - \bar{e}_2 \times \bar{e}_1 \dot{\theta}] \sin^2\theta \right\} d\theta dR_* ds \\
&= \rho \pi \int_0^l \int_0^{\frac{d}{2}} R_*^3 [\bar{e}_1 \times \dot{\bar{e}}_1 + 2 \bar{e}_t \dot{\theta} + \bar{e}_2 \times \dot{\bar{e}}_2] dR_* ds \\
&= \rho \pi \frac{d^4}{32} \int_0^l \left[\frac{1}{2} \bar{e}_1 \times \dot{\bar{e}}_1 + \frac{1}{2} \bar{e}_2 \times \dot{\bar{e}}_2 + \bar{e}_t \dot{\theta} \right] ds \\
\therefore \bar{L} &= \int_0^l [\rho A \bar{r} \times \dot{\bar{r}} + \bar{H}] ds \quad \dots (II.10)
\end{aligned}$$

$$\text{where } \bar{H} = \rho I_p \left[\frac{1}{2} \bar{e}_1 \times \dot{\bar{e}}_1 + \frac{1}{2} \bar{e}_2 \times \dot{\bar{e}}_2 + \bar{e}_t \dot{\theta} \right] \quad \dots (II.11)$$

I_p is the polar moment of inertia $= \pi d^4/32$ for a solid circular cross-section. For a hollow pipe section, the limits of integration would be different from those used in the previous development, but I_p and A in (II.10) and (II.11) would be the polar moment of inertia and Area for that hollow section.

Substituting (II.10) into (II.4) yields

$$\int_0^l \left[\rho A \frac{\partial}{\partial t} (\bar{r} \times \dot{\bar{r}}) + \dot{\bar{H}} \right] ds = \bar{r} \times (\bar{N}_t + \bar{Q}) + \int_0^l \left[\frac{\partial \bar{M}}{\partial s} + \bar{r} \times \bar{f} \right] ds \quad \dots (II.12)$$

In view of (II.9), the first term on the left hand side of (II.12) can be written as

$$\begin{aligned}
\int_0^{\ell} \rho A \frac{\partial}{\partial t} (\bar{\mathbf{r}} \times \dot{\bar{\mathbf{r}}}) ds &= \int_0^{\ell} (\bar{\mathbf{r}} \times \rho A \ddot{\bar{\mathbf{r}}}) ds = \int_0^{\ell} \bar{\mathbf{r}} \times \left[\frac{\partial}{\partial s} (\bar{\mathbf{N}}_t + \bar{\mathbf{Q}}) + \bar{\mathbf{f}} \right] ds \\
&= \int_0^{\ell} \bar{\mathbf{r}} \times \frac{\partial}{\partial s} (\bar{\mathbf{N}}_t + \bar{\mathbf{Q}}) ds + \int_0^{\ell} (\bar{\mathbf{r}} \times \bar{\mathbf{f}}) ds \\
&= \int_0^{\ell} \frac{\partial}{\partial s} \left[\bar{\mathbf{r}} \times (\bar{\mathbf{N}}_t + \bar{\mathbf{Q}}) \right] ds - \int_0^{\ell} \left[\frac{\partial \bar{\mathbf{r}}}{\partial s} \times (\bar{\mathbf{N}}_t + \bar{\mathbf{Q}}) \right] ds + \int_0^{\ell} (\bar{\mathbf{r}} \times \bar{\mathbf{f}}) ds \\
\text{i.e., } \int_0^{\ell} \rho A \frac{\partial}{\partial t} (\bar{\mathbf{r}} \times \dot{\bar{\mathbf{r}}}) ds &= \bar{\mathbf{r}} \times (\bar{\mathbf{N}}_t + \bar{\mathbf{Q}}) - \int_0^{\ell} \left[\bar{\mathbf{e}}_t \times (\bar{\mathbf{N}}_t + \bar{\mathbf{Q}}) - (\bar{\mathbf{r}} \times \bar{\mathbf{f}}) \right] ds \\
&\dots \text{(II.13)}
\end{aligned}$$

Subtracting (II.13) from (II.12) yields

$$\int_0^{\ell} \left[\dot{\bar{\mathbf{H}}} - \frac{\partial \bar{\mathbf{M}}}{\partial s} - \bar{\mathbf{e}}_t \times \bar{\mathbf{Q}} \right] ds = 0 \quad \dots \text{(II.14)}$$

noting that $\bar{\mathbf{e}}_t \times \bar{\mathbf{N}}_t = 0$. In order that (II.14) is satisfied for all values of ℓ , it is required that

$$\dot{\bar{\mathbf{H}}} = \frac{\partial \bar{\mathbf{M}}}{\partial s} + \bar{\mathbf{e}}_t \times \bar{\mathbf{Q}} \quad \dots \text{(II.15)}$$

It is convenient to eliminate the shear force vector $\bar{\mathbf{Q}}$ from (II.9). Using the vector identity $(\bar{\mathbf{e}}_t \times \bar{\mathbf{Q}}) \times \bar{\mathbf{e}}_t = \bar{\mathbf{Q}}$, (II.15) can be written

$$\bar{\mathbf{Q}} = \dot{\bar{\mathbf{H}}} \times \bar{\mathbf{e}}_t + \bar{\mathbf{e}}_t \times \frac{\partial \bar{\mathbf{M}}}{\partial s}$$

and (II.9) becomes

$$\rho A \ddot{\bar{\mathbf{r}}} = \frac{\partial}{\partial s} \left[\bar{\mathbf{N}}_t + \dot{\bar{\mathbf{H}}} \times \bar{\mathbf{e}}_t + \bar{\mathbf{e}}_t \times \frac{\partial \bar{\mathbf{M}}}{\partial s} \right] + \bar{\mathbf{f}} \quad \dots \text{(II.16)}$$

Equations (II.15) and (II.16) will be taken as the equations of motion for the rod under the applied forces.

3. Reduction of Equations of Motions

The position vector \bar{r} for the axis of the rod can be written $\bar{r}(s,t) = \bar{r}_0(s) + \bar{u}(s,t)$, where $\bar{r}_0(s)$ is the position vector denoting the axis of the rod in its unstressed state, and $\bar{u}(s,t)$ is the displacement vector of the rod under load. It is assumed that the displacements of each section of the rod from its unstressed state are small. By imposing that $|\bar{u}(s,t)| \ll |\bar{r}_0(s)|$ for all t and s , approximations can be made that the trihedral \bar{e}_t, \bar{e}_1 and \bar{e}_2 can be determined based on the unstressed configuration \bar{r}_0 instead of \bar{r} . The relationship between the position vector \bar{r}_0 of the space curve and the trihedral is well known. The variation along the length of the axis is given by the Frenet-Serret formulae, which can be stated as

$$\frac{\partial \bar{e}_t}{\partial s} = \kappa_0 \bar{e}_1$$

$$\frac{\partial \bar{e}_1}{\partial s} = -\kappa_0 \bar{e}_t + \tau_0 \bar{e}_2$$

$$\frac{\partial \bar{e}_2}{\partial s} = -\tau_0 \bar{e}_1$$

where κ_0 is the curvature and τ_0 is the tortuosity of the centerline of the rod. A summary of useful relations is given in the Appendix (A.I.1) to (A.I.11). If the trihedral is defined based on \bar{r}_0 as shown in the appendix, then it is a function of s only, and is independent of time t . Therefore, any time derivatives of the trihedral

will be zero due to the assumption of small motions of the rod. Using the relations given in the Appendix, each term of (II.15) and (II.16) can be written explicitly in terms of components in the \bar{e}_t , \bar{e}_1 and \bar{e}_2 directions.

From (II.11) and (II.15)

$$\dot{\bar{H}} = \rho I_p \ddot{\theta} \bar{e}_t = \frac{\partial \bar{M}}{\partial s} + \bar{e}_t \times \bar{Q}$$

where

$$\bar{M} = M_1 \bar{e}_1 + M_2 \bar{e}_2 + M_t \bar{e}_t$$

and

$$\bar{Q} = Q_1 \bar{e}_1 + Q_2 \bar{e}_2$$

$$\begin{aligned} \therefore \rho I_p \ddot{\theta} \bar{e}_t &= \frac{\partial M_1}{\partial s} \bar{e}_1 + \frac{\partial M_2}{\partial s} \bar{e}_2 + \frac{\partial}{\partial s} M_t \bar{e}_t + M_1 \left[\tau_0 \bar{e}_2 - \kappa_0 \bar{e}_t \right] \\ &\quad - M_2 \tau_0 \bar{e}_1 + M_t \kappa_0 \bar{e}_1 + Q_1 \bar{e}_2 - Q_2 \bar{e}_1 \end{aligned}$$

Defining $U_\theta \equiv \theta$, and equating coefficients in the three directions yields

$$\rho I_p a \ddot{U}_\theta = M_t' - \kappa M_1 \quad \dots (II.18)$$

$$a Q_2 = M_1' - \tau M_2 + \kappa M_t \quad \dots (II.19)$$

$$a Q_1 = -\tau M_1 - M_2' \quad \dots (II.20)$$

where $()' = \frac{\partial}{\partial \xi} ()$ etc., $\xi = s/a$, and a is the radius of gyration of the rod. κ and τ are the non-dimensional curvature and tortuosity of the space curve given by $\kappa = a \kappa_0$ and $\tau = a \tau_0$. The radius of gyration of the rod is used throughout this thesis as the characteristic

length for purposes of normalisation.

Since $\dot{\bar{H}} \times \bar{e}_t = 0$, (II.16) becomes

$$\rho A \bar{r} = \frac{\partial}{\partial s} \left[\bar{N}_t + \bar{e}_t \times \frac{\partial \bar{M}}{\partial s} \right] + \bar{f}$$

But,

$$\begin{aligned} \bar{N}_t + \bar{e}_t \times \frac{\partial \bar{M}}{\partial s} &= N_t \bar{e}_t + \bar{e}_t \times \left[\frac{\partial M_1}{\partial s} \bar{e}_1 + \frac{\partial M_2}{\partial s} \bar{e}_2 + \frac{\partial M_t}{\partial s} \bar{e}_t \right. \\ &\quad \left. + M_1 (\tau_o \bar{e}_2 - \kappa_o \bar{e}_t) - M_2 \tau_o \bar{e}_1 + M_t \kappa_o \bar{e}_1 \right] \\ &= N_t \bar{e}_t + \left[\frac{\partial M_1}{\partial s} - M_2 \tau_o + M_t \kappa_o \right] \bar{e}_2 - \left[\frac{\partial M_2}{\partial s} + M_1 \tau_o \right] \bar{e}_1 \end{aligned}$$

Letting $\bar{u}(s,t) = u_1(s,t) \bar{e}_1 + u_2(s,t) \bar{e}_2 + u_t(s,t) \bar{e}_t$

$$\begin{aligned} \text{then } \rho A (\ddot{u}_1 \bar{e}_1 + \ddot{u}_2 \bar{e}_2 + \ddot{u}_t \bar{e}_t) &= \frac{\partial}{\partial s} \left[N_t \bar{e}_t + \left(\frac{\partial M_1}{\partial s} - M_2 \tau_o + M_t \kappa_o \right) \bar{e}_2 \right. \\ &\quad \left. - \left(\frac{\partial M_2}{\partial s} + M_1 \tau_o \right) \bar{e}_1 \right] + \bar{f} \end{aligned}$$

Carrying out the differentiation and equating coefficients in the three directions, yields

$$\rho A a^3 \ddot{U}_t = a N'_t + \kappa \tau M_1 + \kappa M'_2 + a^2 f_t \quad \dots (II.21)$$

$$\begin{aligned} \rho A a^3 \ddot{U}_1 &= a \kappa N_t - \kappa \tau M_t - 2 \tau M'_1 - M_1 \tau' + \tau^2 M_2 - M_2' + a^2 f_1 \\ &\quad \dots (II.22) \end{aligned}$$

$$\begin{aligned} \rho A a^3 \ddot{U}_2 &= \kappa M'_t + M_t \kappa' + M_1' - \tau^2 M_1 - 2 \tau M'_2 - M_2 \tau' + a^2 f_2 \\ &\quad \dots (II.23) \end{aligned}$$

where $\bar{U} = \bar{u}/a = U_t \bar{e}_t + U_1 \bar{e}_1 + U_2 \bar{e}_2$

Equations (II.18) to (II.20) are the equations pertaining to the rotational equilibrium of the rod, as they are derived from (II.15). Equations (II.21) to (II.23) are

equilibrium equations for the translation of an element of the rod obtained from equation (II.16). (II.19) and (II.20) are expressions for the transverse shear forces Q_1 and Q_2 in terms of the moments. In a similar manner, equations (II.18), (II.21), (II.22) and (II.23) express the dimensionless displacement variables U_θ , U_t , U_1 and U_2 in terms of moments and applied loadings.

4. Generalised Force-Displacement Relationships

In order to express equations (II.18) to (II.23) in terms of displacement variables, it is necessary to obtain the generalised force-displacement relationships. These are given by Love⁵, and the derivations are given in Appendix (A.V). They can be written as

$$a M_t = GI_p (U_\theta' + \kappa\tau U_1 + \kappa U_2') \quad \dots (II.24)$$

$$a M_1 = EI (\kappa U_\theta - \tau\kappa U_t - 2\tau U_1' - \tau' U_1 + \tau^2 U_2 - U_2'') \quad \dots (II.25)$$

$$a M_2 = EI (\kappa U_t' + \kappa' U_t + U_1'' - \tau^2 U_1 - 2\tau U_2' - \tau' U_2) \quad \dots (II.26)$$

$$N_t = EA (U_t' - \kappa U_1) \quad \dots (II.27)$$

Substituting (II.24) to (II.26) into (II.19) and (II.20), the transverse shear forces Q_1 and Q_2 may be expressed in terms of the generalised displacements U_θ , U_t , U_1 and U_2 . Substituting (II.24) to (II.27) into (II.18), (II.21), (II.22) and (II.23), four equations of

motion of the rod are obtained in terms of the displacement variables and applied loadings.

5. Four Equations of Motion in Terms of Displacement Variables

Substituting for M_t , M_1 , M_2 , N_t and their derivatives where applicable as given by (II.24) to (II.27), the four equations of motion in terms of displacement variables U_θ , U_t , U_1 and U_2 are developed.

Equation (II.18) becomes

$$\frac{2\rho a^2}{E} \ddot{U}_\theta = \frac{2G}{E} \left[U'_\theta + (\kappa'\tau + \kappa\tau')U_1 + \kappa\tau U'_1 + \kappa'U'_2 + \kappa U''_2 \right] - \kappa[\kappa U_\theta - \tau\kappa U_t - 2\tau U'_1 - \tau'U_1 + \tau^2 U_2 - U_2''] \quad \dots (II.28)$$

Equation (II.21) becomes

$$\begin{aligned} \rho I a \ddot{U}_t = & aEA(U'_t - \kappa'U_1 - \kappa U'_1) + \kappa\tau \frac{EI}{a} (\kappa U_\theta - \kappa\tau U_t - 2\tau U'_1 - \tau'U_1 + \tau^2 U_2 - U_2'') \\ & + \frac{\kappa EI}{a} (2\kappa'U'_t + \kappa U''_t + \kappa''U_t - 2\tau\tau'U_1 - \tau^2 U'_1 + U_1'' - \tau''U_2 \\ & - 3\tau'U'_2 - 2\tau U_2'') + a^2 f_t \quad \dots (II.29) \end{aligned}$$

Equation (II.22) becomes

$$\begin{aligned} \rho I a \ddot{U}_1 = & a\kappa EA(U'_t - \kappa U_1) - \frac{\kappa\tau GI}{a} P (U'_\theta + \kappa\tau U_1 + \kappa U'_2) \\ & - \frac{2\tau EI}{a} (\kappa'U_\theta + \kappa U'_\theta - \tau'\kappa U_t - \tau\kappa'U_t - \tau\kappa U'_t - 2\tau'U'_1 - 2\tau U_1'' - \tau''U_1 \\ & - \tau'U'_1 + 2\tau\tau'U_2 + \tau^2 U_2 - U_2'') \\ & - \frac{\tau'EI}{a} (\kappa U_\theta - \tau\kappa U_t - 2\tau U'_1 - \tau'U_1 + \tau^2 U_2 - U_2'') \\ & + \frac{\tau^2 EI}{a} (\kappa U'_t + \kappa'U_t + U_1'' - \tau^2 U_1 - 2\tau U_2' - \tau'U_2) \end{aligned}$$

$$\begin{aligned}
& - \frac{EI}{a} \left[\kappa U_t'' + 3\kappa' U_t' + 3\kappa'' U_t + \kappa''' U_t + U_1'''' - \tau^2 U_1' - 4\tau\tau' U_1' \right. \\
& \quad \left. - (2\tau'\tau' + 2\tau\tau'') U_1 \right. \\
& \quad \left. - 2\tau U_2'' - 5\tau' U_2' - 4\tau'' U_2 - \tau''' U_2 \right] + a^2 f_1 \\
& \quad \dots (II.30)
\end{aligned}$$

and equation (II.23) becomes

$$\begin{aligned}
\rho I a \ddot{U}_2 &= \frac{\kappa G I_P}{a} \left[U_\theta' + (\kappa'\tau + \kappa\tau') U_1 + \kappa\tau U_1' + \kappa' U_2' + \kappa U_2'' \right] + \frac{\kappa' G I_P}{a} (U_\theta' + \kappa\tau U_1 + \kappa U_2') \\
&+ \frac{EI}{a} \left[\kappa U_\theta'' + 2\kappa' U_\theta' + \kappa'' U_\theta - \kappa\tau U_t' - (2\tau\kappa' + 2\tau'\kappa) U_t' \right. \\
& \quad \left. - (\tau''\kappa + \tau\kappa'' + 2\tau'\kappa') U_t \right. \\
& \quad \left. - 2\tau U_1'' - 5\tau' U_1' - 4\tau'' U_1 - \tau''' U_1 + \tau^2 U_2' + 4\tau\tau' U_2' \right. \\
& \quad \left. + (2\tau'\tau' + 2\tau\tau'') U_2 - U_2'''' \right] \\
&- \frac{\tau^2 EI}{a} (\kappa U_\theta - \tau\kappa U_t - 2\tau U_1' - \tau' U_1 + \tau^2 U_2 - U_2') \\
&- \frac{2\tau EI}{a} (2\kappa' U_t' + \kappa U_t'' + \kappa'' U_t - 2\tau\tau' U_1 - \tau^2 U_1' + U_1'' - \tau' U_2 - 3\tau' U_2' - 2\tau U_2'') \\
&- \frac{\tau' EI}{a} (\kappa U_t' + \kappa' U_t + U_1' - \tau^2 U_1 - 2\tau U_2' - \tau' U_2) + a^2 f_2 \quad \dots (II.31)
\end{aligned}$$

Subjected to the appropriate boundary and initial conditions, the motion of the rod can be studied using equations (II.28) to (II.31), the four equations of motion. These equations are useful in studying the behaviour of a rod of circular cross section, the axis of which is in the form of any general space curve. It should be pointed out that these equations are indeed lengthy and complicated. In order to solve them, $\kappa(\xi)$ and $\tau(\xi)$ must be known for a

general space curve, and this in itself may be a difficult problem. Numerical methods and the point by point measurement of κ and τ along the space curve may be necessary.

CHAPTER III

DYNAMIC EQUATIONS OF MOTION OF A HELICAL SPRING

1. Introduction

Equations (II.28) to (II.31) developed in Chapter II will now be used to study the dynamic behaviour of some special systems.

One simple configuration of a naturally curved and twisted rod is in the form of a helix, in which both the curvature κ and the tortuosity τ of the axis are constants. In order to solve the problem of a helical spring under an external forcing function, it is necessary to solve the free vibrational problem. The equations for the free vibrations of a helical rod can be obtained from (II.28) to (II.31) by setting any derivatives of κ and τ equal to zero, and neglecting the applied loading terms. In matrix notation, the resulting equations can be written as

$$\begin{bmatrix} 1 & 0 & 0 & 0 \\ 0 & 1 & 0 & 0 \\ 0 & 0 & 1 & 0 \\ 0 & 0 & 0 & 2 \end{bmatrix} \begin{Bmatrix} \ddot{U}_t \\ \ddot{U}_1 \\ \ddot{U}_2 \\ \ddot{U}_\theta \end{Bmatrix} = \frac{E}{\rho a^2} \begin{bmatrix} \gamma_{11} & \gamma_{12} & \gamma_{13} & \gamma_{14} \\ -\gamma_{12} & \gamma_{22} & \gamma_{23} & \gamma_{24} \\ \gamma_{13} & -\gamma_{23} & \gamma_{33} & \gamma_{34} \\ \gamma_{14} & -\gamma_{24} & \gamma_{34} & \gamma_{44} \end{bmatrix} \begin{Bmatrix} U_t \\ U_1 \\ U_2 \\ U_\theta \end{Bmatrix}$$

... (III.1)

where the $[\gamma]$ matrix contains differential operators as elements given by

$$\gamma_{11} = D_2(1+\kappa^2) - \kappa^2\tau^2 \quad \dots(\text{III.2a})$$

$$\gamma_{12} = \kappa[D_3 - (1+3\tau^2)D] \quad \dots(\text{III.2b})$$

$$\gamma_{13} = \kappa\tau(\tau^2 - 3D_2) \quad \dots(\text{III.2c})$$

$$\gamma_{14} = \kappa^2\tau \quad \dots(\text{III.2d})$$

$$\gamma_{22} = -D_4 - \kappa^2 + \tau^2 \left[6D_2 - \left(\frac{2G}{E} \kappa^2 + \tau^2 \right) \right] \quad \dots(\text{III.2e})$$

$$\gamma_{23} = 2\tau \left[2D_3 - \left(\frac{G}{E} \kappa^2 + 2\tau^2 \right) D \right] \quad \dots(\text{III.2f})$$

$$\gamma_{24} = -2\kappa\tau \left(1 + \frac{G}{E} \right) D \quad \dots(\text{III.2g})$$

$$\gamma_{33} = -D_4 + \left(\frac{2G}{E} \kappa^2 + 6\tau^2 \right) D_2 - \tau^4 \quad \dots(\text{III.2h})$$

$$\gamma_{34} = \kappa \left[\left(1 + \frac{2G}{E} \right) D_2 - \tau^2 \right] \quad \dots(\text{III.2i})$$

$$\gamma_{44} = \frac{2G}{E} D_2 - \kappa^2 \quad \dots(\text{III.2j})$$

where $D = \frac{\partial}{\partial \xi}$, $D_2 = \frac{\partial^2}{\partial \xi^2}$ etc.

It is advantageous to represent the equations of motion in the form of (III.1) since the coupling among the displacement variables can be recognized easily. This coupling is represented by the off-diagonal terms in the $[\gamma]$ matrix.

The four displacement variables U_t , U_1 , U_2 and U_θ can be considered as generalised coordinates representing

longitudinal motion, transverse motion in two perpendicular directions, and torsional motion of the rod respectively. It can be seen that in the general case of a rod possessing both curvature and tortuosity, all four types of motions will be coupled together.

In general, κ will be small compared to unity, and powers of κ can therefore be neglected in comparison with unity. Also when the pitch angle α is less than 60° , the tortuosity τ is of the same order of magnitude as κ , and higher powers of τ can also be neglected in comparison with unity.

2. Wave Propagation along a Helical Spring

Consider the case of a sinusoidal wave train propagating along a curved rod in the form of a helical spring. Let the spring have a pitch angle α , radius R , cross-sectional diameter d as shown in figure III.1. No reflection of the stress wave from the ends of the spring are considered. In this respect, the helical spring can be considered infinitely long.

The normalised curvature and tortuosity of the spring in terms of the coil dimensions are given by

$$\kappa = \frac{a}{R} \cos^2 \alpha \quad \dots(\text{III.3})$$

$$\tau = \kappa \tan \alpha$$

The equations of motion (III.1) apply in this case. Investigate the propagation of a sinusoidal wave

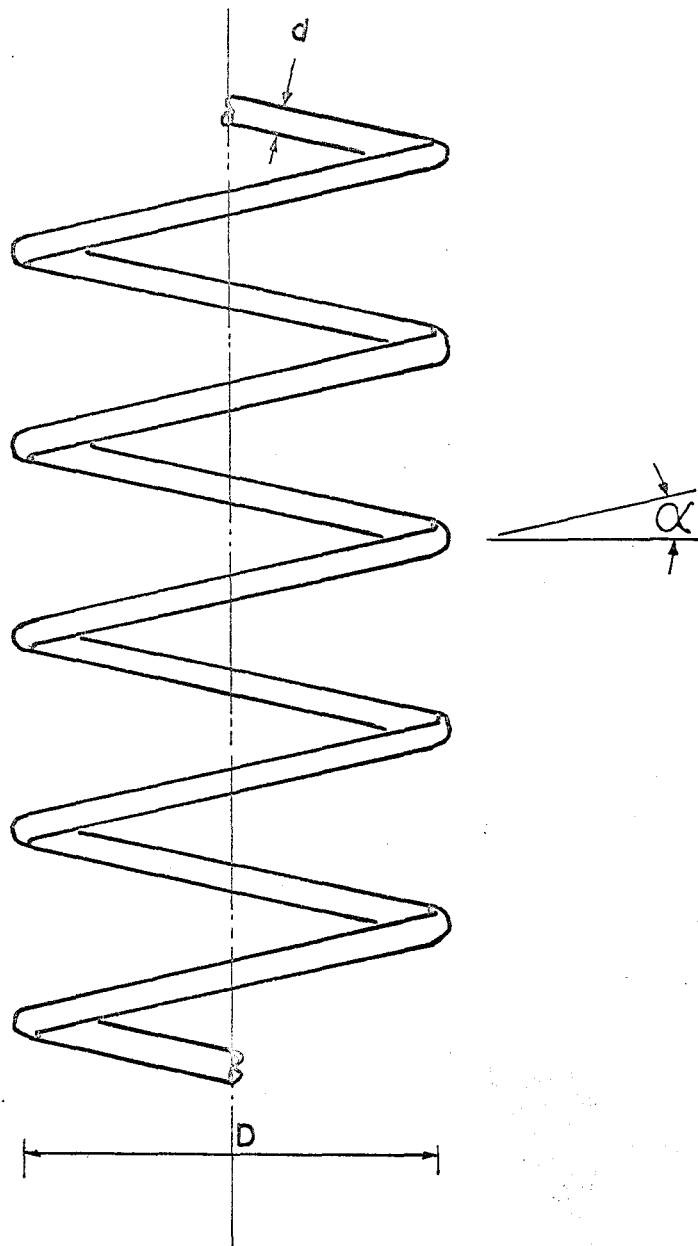


FIG III.1 HELICAL SPRING

train of the form

$$\left\{ \eta \right\} = \begin{Bmatrix} U_t \\ U_1 \\ U_2 \\ U_\theta \end{Bmatrix} = \begin{Bmatrix} \eta_t \sin \lambda \xi \\ \eta_1 \cos \lambda \xi \\ \eta_2 \sin \lambda \xi \\ \eta_\theta \sin \lambda \xi \end{Bmatrix} \sin \omega t \quad \dots \text{(III.4)}$$

$$\text{where } \lambda = \pi a / \ell \quad \dots \text{(III.4a)}$$

η_t , η_1 , η_2 and η_θ are constants representing the amplitudes of axial, transverse in-plane, transverse out-of-plane and torsional motions respectively. Equations (III.4) represent a harmonic wave train of wavelength $2\pi/\lambda$ with a wave velocity of ω/λ .

It can be seen that a sinusoidal wave of the form given in (III.4) satisfies the following conditions, namely, at $\xi = 0$ and ℓ/a .

$$U_t = U_1' = U_1''' = U_2 = U_2' = U_\theta = 0 \quad \dots \text{(III.4b)}$$

Therefore, the problem of studying the wavelength and wave velocity relationship for the propagation of a sinusoidal wave of the form given by (III.4) is equivalent to the study of the natural frequencies of a helical spring of finite length ℓ supported at the ends $\xi = 0$ and $\xi = \ell/a$ such that conditions (III.4b) are satisfied. For convenience of visualisation, the latter terminology will be used, and the natural frequencies of a finite helical spring of length ℓ subjected to boundary conditions (III.4b) will be investigated in detail.

Substituting equations (III.4) into (III.1) yields

$$\begin{bmatrix} \beta_{11} - \Omega^2 & \beta_{12} & \beta_{13} & \beta_{14} \\ \beta_{12} & \beta_{22} - \Omega^2 & \beta_{23} & \beta_{24} \\ \beta_{13} & \beta_{23} & \beta_{33} - \Omega^2 & \beta_{34} \\ \beta_{14} & \beta_{24} & \beta_{34} & \beta_{44} - 2\Omega^2 \end{bmatrix} \begin{Bmatrix} n_t \\ n_1 \\ n_2 \\ n_\theta \end{Bmatrix} = \begin{Bmatrix} 0 \\ 0 \\ 0 \\ 0 \end{Bmatrix} \quad \dots \text{(III.5)}$$

where $\Omega^2 \equiv \omega^2 \rho a^2 / E$... (III.6)

$$\beta_{11} = \lambda^2 (1 + \kappa^2) + \kappa^2 \tau^2 \quad \dots \text{(III.7a)}$$

$$\beta_{12} = -\lambda \kappa (\lambda^2 + 1 + 3\tau^2) \quad \dots \text{(III.7b)}$$

$$\beta_{13} = -\kappa \tau (\tau^2 + 3\lambda^2) \quad \dots \text{(III.7c)}$$

$$\beta_{14} = -\kappa^2 \tau \quad \dots \text{(III.7d)}$$

$$\beta_{22} = \lambda^4 + \kappa^2 + \tau^2 (6\lambda^2 + \frac{2G}{E} \kappa^2 + \tau^2) \quad \dots \text{(III.7e)}$$

$$\beta_{23} = 2\lambda \tau (2\lambda^2 + \frac{G}{E} \kappa^2 + 2\tau^2) \quad \dots \text{(III.7f)}$$

$$\beta_{24} = 2\lambda \kappa \tau (1 + \frac{G}{E}) \quad \dots \text{(III.7g)}$$

$$\beta_{33} = \lambda^4 + \tau^4 + 2\lambda^2 (\frac{G}{E} \kappa^2 + 3\tau^2) \quad \dots \text{(III.7h)}$$

$$\beta_{34} = \lambda^2 \kappa (1 + \frac{2G}{E}) + \kappa \tau^2 \quad \dots \text{(III.7i)}$$

$$\beta_{44} = \frac{2G}{E} \lambda^2 + \kappa^2 \quad \dots \text{(III.7j)}$$

For any given helical spring, the parameters κ, τ and λ and hence the $[\beta]$ matrix can be evaluated using (III.3) to (III.5). Equations (III.5) yield four eigenvalues Ω_i^2 and the associated eigenvectors

$$\left\{ n \right\}_i, \quad (i = 1, 2, 3, 4)$$

A typical set of values of the eigenvectors and natural frequencies is shown in Table III.1. The natural frequencies ω_i , ($i = 1, 2, 3, 4$) are obtained from (III.6) for each of the eigenvalues Ω_i^2 , ($i = 1, 2, 3, 4$) obtained.

For example, consider the case of the helical spring of five turns. The associated eigenvector for the frequency of 90.69 cycles per second is given by (1.0, 0.101, -0.332, 0.007). Elements in the eigenvector indicate that, associated with this natural frequency, the mode of vibration consists of mainly displacement in the tangential direction. The displacements U_1 , U_2 and U_θ are small compared with U_t in this mode.

TABLE III.1

Spring Data: $R=1.52"$; $d=0.266"$; $\rho=0.734 \times 10^{-3} \text{ lb sec}^2/\text{in.}^4$ $\alpha=8.4^\circ$; $E=30 \times 10^6 \text{ psi}$; $G=12 \times 10^6 \text{ psi}$.

No. of Turns N	Associated Eigenvectors				Natural Frequencies c.p.s.			
	η_t	η_1	η_2	η_θ	ω_1	ω_2	ω_3	ω_4
5.0	1	0.101	-0.332	0.007	90.69	20,868.	81.05	14,741.
	-0.101	1	*	0.002				
	0.329	-0.033	1	*				
	-0.012	-0.006	0.003	1				
2.0	1	0.253	-0.503	0.008	210.80	21,416.	186.52	15,052.
	-0.253	1	*	0.006				
	0.473	0.119	1	-0.003				
	-0.007	-0.013	0.011	1				
1.5	1	0.337	-0.663	0.010	263.28	21,911.	229.00	15,334.
	-0.337	1	*	0.007				
	0.595	0.201	1	-0.007				
	-0.003	-0.015	0.018	1				
1.1	1	0.460	-0.954	0.016	316.56	22,853.	261.29	15,875.
	-0.460	1	*	0.009				
	0.788	0.362	1	-0.013				
	0.003	-0.016	0.029	1				
1.0	-0.930	-0.471	1	-0.019	328.87	23,368.	263.11	16,115.
	-0.506	1	*	0.009				
	0.856	0.433	1	-0.016				
	0.005	-0.016	0.034	1				
0.9	0.936	0.526	1	-0.020	257.30	23,819.	337.95	16,434.
	-0.562	1	0.001	0.010				
	-0.813	-0.457	1	-0.021				
	0.007	-0.014	0.040	1				
0.6	1	0.842	0.644	-0.027	103.42	27,166.	289.30	18,403.
	-0.842	1	0.001	0.011				
	-0.378	-0.319	1	-0.034				
	0.015	-0.009	0.071	1				
0.5	1	-0.990	-0.002	-0.011	29,551.	1.044**	267.16	19,828.
	0.990	1	-0.146	*				
	0.073	0.073	1	-0.044				
	0.017	-0.004	0.088	1				
0.4	1	-0.793	-0.002	-0.008	33,504.	238.77	641.73	22,219.
	0.792	1	-0.991	0.046				
	0.486	0.612	1	-0.059				
	0.018	0.001	0.109	1				
($\alpha=0^\circ$)								
0.5	1	1	0	0	2.6**	30,027.	0.340**	20,162.
	-1	1	0	0				
	0	0	1	-0.044				
	0	0	0.088	1				

**" indicates that the absolute value of the entry is less than 0.001.

***" indicates that these values are approximately equal to zero.

The calculations in Table III.1 were done on the IBM 7040 Electronic Digital Computer using the Jacobi Rotations Method⁶. Essentially, the method transforms the [B] matrix into a diagonal matrix. The eigenvalue Ω_1^2 is obtained from the first element of this diagonal matrix, Ω_2^2 is obtained from the second element and so on.

It is noticed that two of the frequencies are lower than the remaining two by orders of magnitude. For a helical spring with the number of turns N less than one half, both the in-plane and out-of-plane bending stiffnesses are much less than the extensional and torsional stiffnesses. Hence, the two lower frequencies are associated with flexural vibrations.

For a spring with N greater than unity, Table III.1 shows that the element n_t in a mode associated with one of the two smaller values of natural frequencies is always numerically larger than the other three elements, indicating that the mode of vibration consists mainly of longitudinal movements. This can be explained by observing that a "long" spring of this kind is relatively flexible if it is rotated about its coiled axis. If the spring is vibrating at a frequency ω_1 , the lowest of the natural frequencies, then the elements of the spring are subjected mainly to longitudinal movements, resulting in a relative rotation between the top and bottom of the spring about the coiled axis. For a "long" spring, this mode of deformation offers less

rigidity than the in-plane flexural deformation, and hence such a mode is associated with a lower natural frequency. Wittrick² has shown that this is true for in-plane deformation of long springs, by pointing out that the kinetic energy associated with the longitudinal direction is numerically larger than the energies associated with the other directions.

For a spring with N between one half and unity, the coupling between the in-plane transverse motion and longitudinal motion becomes strong, and it is difficult to identify which type of motion predominates in the vibrational mode.

Wittrick² has shown that for out-of-plane deformation, the kinetic energy associated with the out-of-plane direction is numerically greater than the energies associated with the other directions. This can be seen in Table III.1, where, for all lengths of spring considered, η_2 is numerically the largest component of the eigenvector associated with the other low value of natural frequency. This indicates that the frequency ω_3 in Table III.1 is always associated with the out-of-plane flexural vibration mode of the spring.

In his investigation¹, Love has neglected torsional inertia of the rod, and has assumed that the axis of the rod is inextensible. The latter assumption implies that the axial strain at the axis, and hence the axial force N_t , is zero. The two assumptions can be expressed mathematically

as

$$I_p \ddot{U}_\theta = 0$$

and from (II.27) $U'_t = \kappa U_1$

If these assumptions are introduced into (III.1), the resulting frequency equation as given by Love¹ becomes

$$C_1 \Omega^4 - C_2 \Omega^2 + C_3 = 0 \quad \dots \text{(III.8)}$$

where $C_1 = (\lambda^2 + \kappa^2) (\lambda^2 + \frac{E}{2G} \kappa^2)$

$$C_2 = \left[2\lambda^4 + \lambda^2 \kappa^2 \left(1 + \frac{E}{2G} \right) \right] [\lambda^2 - \kappa^2 + \tau^2]^2 + 4\tau^2 \lambda^2 \left[(\lambda^2 - \kappa^2)^2 + C_1 \right]$$

$$C_3 = \lambda^4 (\lambda^2 - \kappa^2 - \tau^2)^4$$

Equation (III.8) is essentially a bi-quadratic in Ω^2 and can be readily solved to yield the two frequencies. The accuracy of (III.8) will be discussed in a later section.

The spectrum curves are plotted for various helical spring parameters and are shown in figures (III.2a, b, c, d).

3. Discussion of Spectrum Curves

The spectrum curves of figures (III.2a, b, c, d) show the variation of the two lowest frequencies as determined from equation (III.5), with respect to length of the helical spring. The curves are shown for varying pitch angle α , and R/a , the normalised radius of the coil spring. The normalised curvature and tortuosity for any of the springs considered are obtained from (III.3). It is shown that as

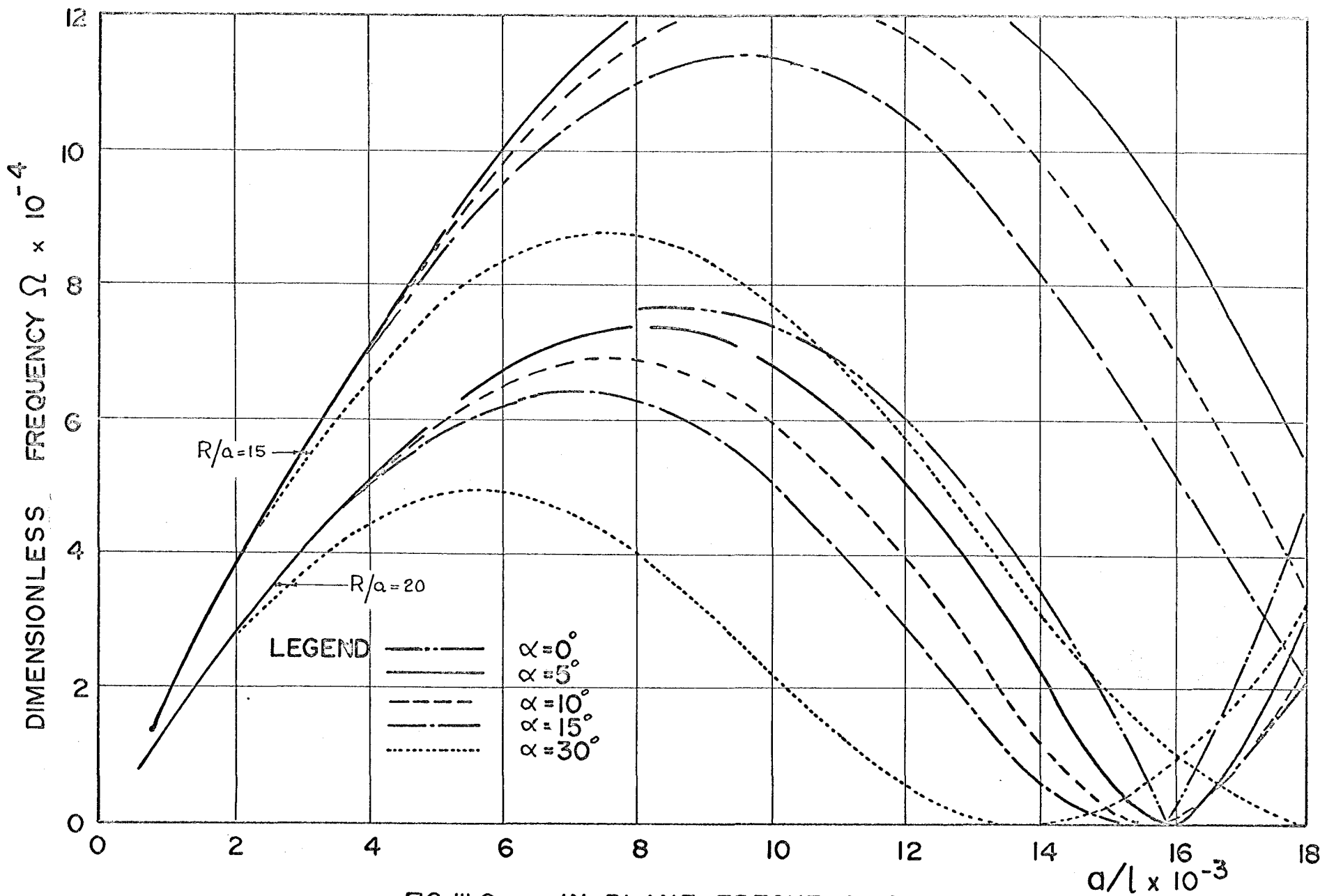


FIG III.2 a IN-PLANE FREQUENCIES

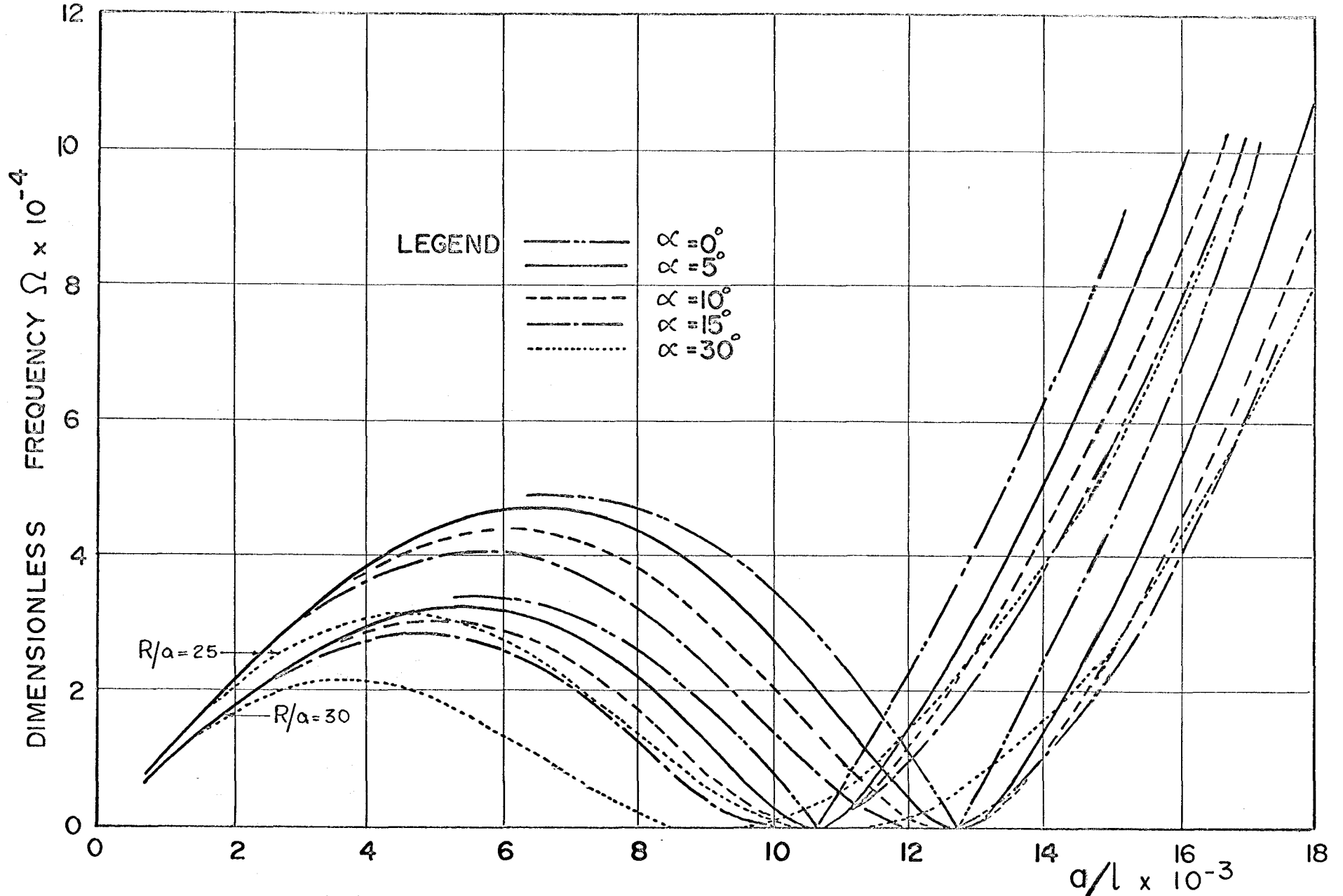
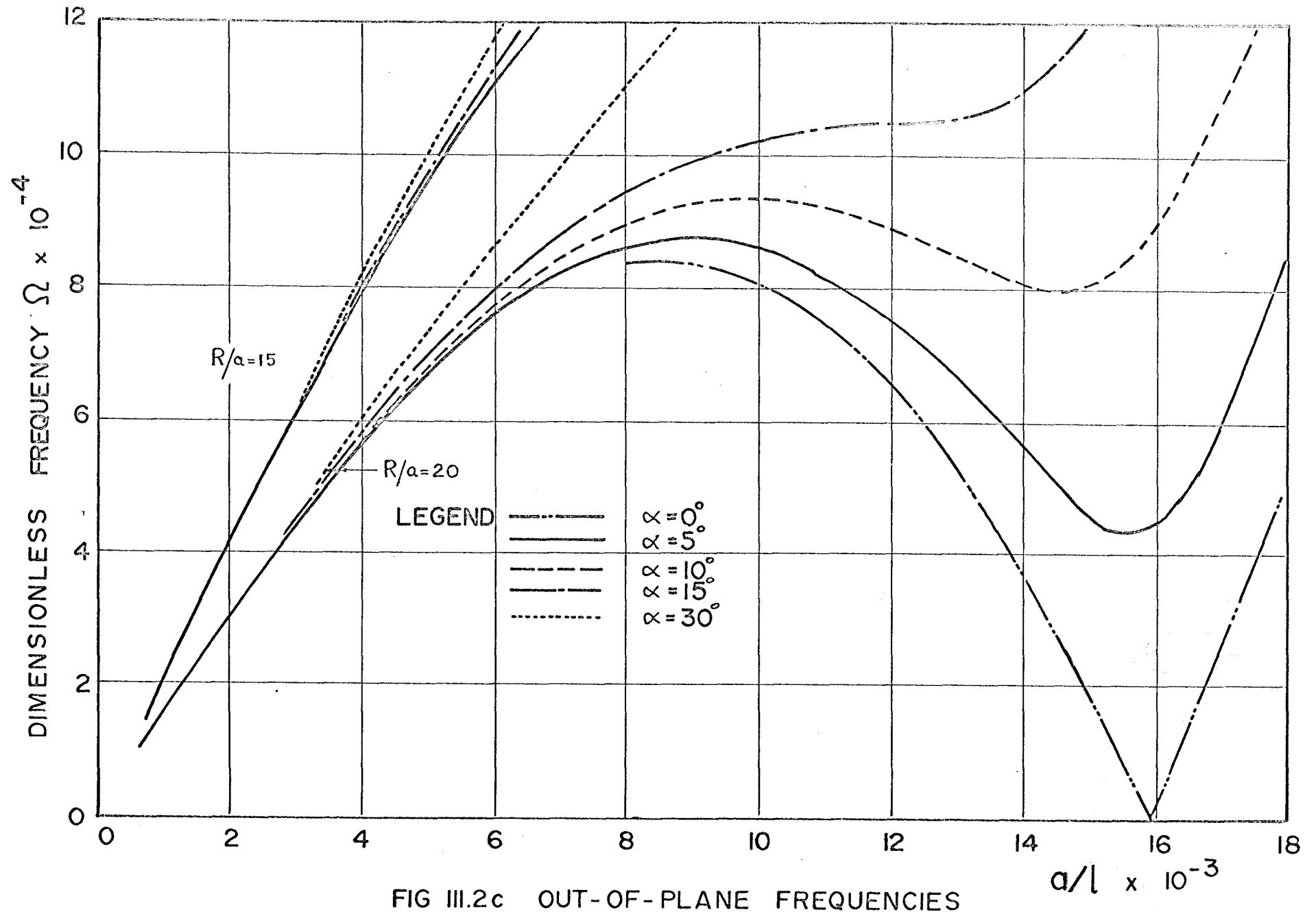


FIG III.2 b IN- PLANE FREQUENCIES



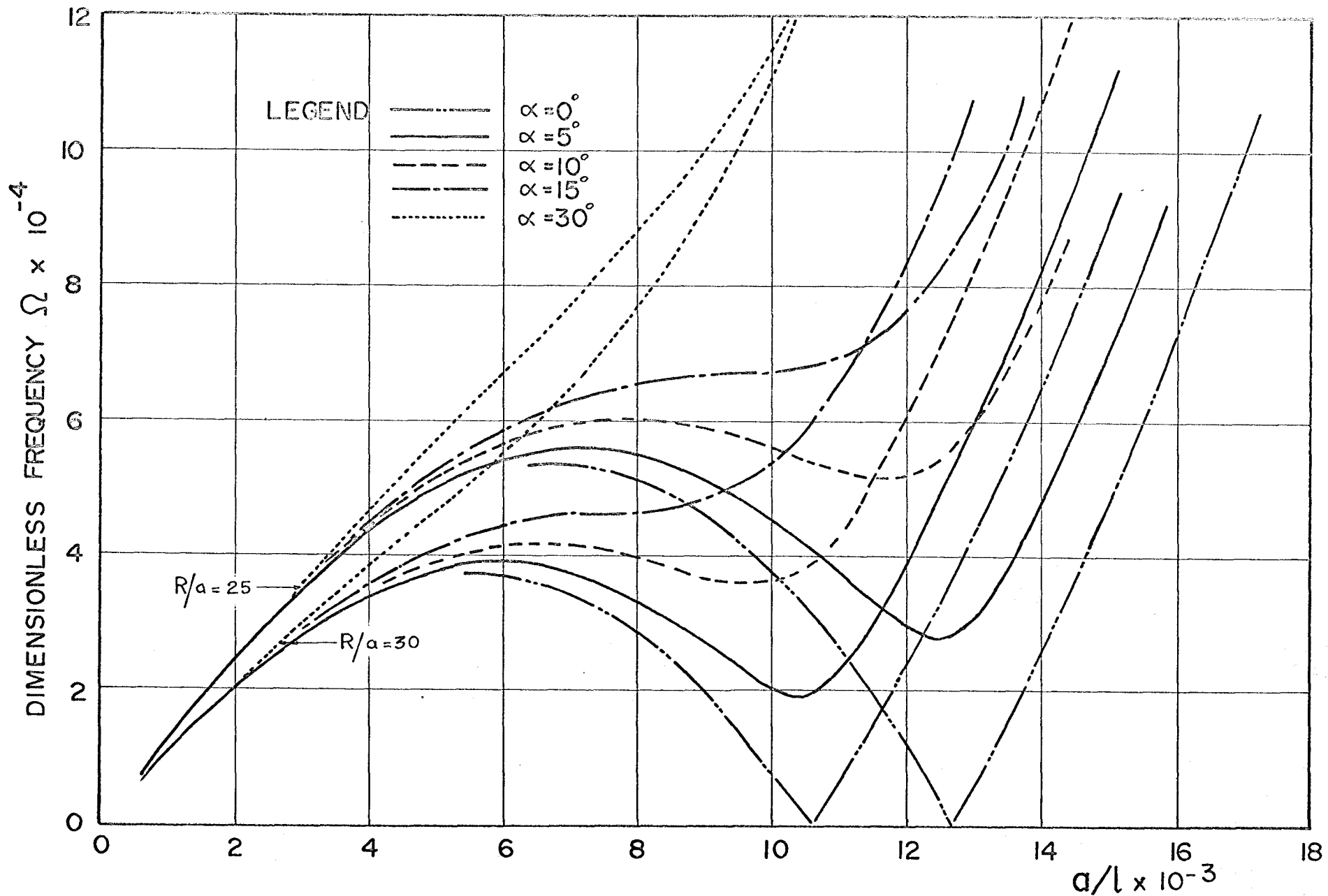


FIG III.2d OUT-OF-PLANE FREQUENCIES

$l \rightarrow \infty$, i.e., for very long springs both frequencies approach zero value. Figures (III.2a, b) show the in-plane frequency variation, and figures (III.2c, d) show the out-of-plane frequency variation with respect to length of helical spring.

An examination of figures III.2a, b shows that when the number of turns N of the helical spring is one half, the in-plane frequency is zero. This is independent of R/a and α . The zero frequency arises because rigid body motion is possible, and each element of the spring moves in planes parallel to each other. As N decreases from infinity to unity, the frequency increases, the greater the curvature, the greater is the rate of increase. It is interesting to note that the frequency attains a maximum value when N is approximately equal to unity. As N decreases further from unity to one half, the frequency decreases, until it is zero at one-half turn. The frequency increases once more as N is decreased from one half, and as N approaches zero, the frequency approaches infinite value.

The zero frequency at infinite length is reasonable, because the rigidity of the spring at this length is small. It was pointed out in section III.2 that it was relatively easy to rotate a long spring about its coil axis by twisting, thus causing predominantly longitudinal motion of the spring elements. It should be noted that the longitudinal direction for any element lies in the plane of the

spring at that point. As N decreases towards unity, the rigidity of the spring against this type of deformation increases, and hence the frequency increases.

The zero frequency at one half turn can be demonstrated by considering the special case when the "spring" is a semi-circular arch. The eigenvector $(1, 1, 0, 0)$ shown in Table III.1 for $N = 0.5$, $\alpha = 0^\circ$, corresponds to this type of in-plane deformation. From (III.4), the mode shape is given by

$$\begin{Bmatrix} \eta_t \text{ Sin } \left(\frac{\pi a}{\ell} \xi \right) \\ \eta_1 \text{ Cos } \left(\frac{\pi a}{\ell} \xi \right) \end{Bmatrix} = \begin{Bmatrix} \text{Sin } \left(\frac{\pi a}{\ell} \xi \right) \\ \text{Cos } \left(\frac{\pi a}{\ell} \xi \right) \end{Bmatrix}$$

since $\eta_t = \eta_1 = 1$.

If the mode shape is determined by plotting the deformation of each point on the arch from $\xi = 0$ to $\xi = \ell/a$, it will be found that rigid body motion has taken place in the plane of the arch. The zero frequency at one half turn of helical spring does not however depend on the value of α . It is shown in the appendix (A.II) that C_3 in (III.8) is zero at one half turn, thus yielding a zero frequency from Love's frequency equation. As N is further decreased from one half, the frequency increases.

Figures (III.2c, d) show the variation of the out-of-plane flexural frequency with respect to length of spring. As ℓ approaches infinite value, the frequency

approaches zero value. As ℓ decreases the frequency increases, the smaller the curvature, the greater the increase. The curves show a drop in frequency for low pitch angles when the length of the spring is such that the number of turns lies between one half and unity. For ring segments, $\alpha=0^\circ$, the frequency drops to zero at one-half turn.

The zero frequency at infinite length is reasonable because the rigidity of the spring at that length is negligible. It is relatively easy to compress a long spring, thereby causing the spring elements to move predominantly in their out-of-plane directions. As ℓ decreases, it becomes more difficult to do so, and therefore the frequency rises. For low pitch angle springs, and if the spring is supported at its ends such that equations (III.4b) are satisfied, it becomes relatively easy to deflect the spring in the out-of-plane direction if the number of turns is approximately one half. In the limit, for $\alpha=0^\circ$, rigid body motion is possible when N is one half. It is shown in appendix (A.III), that C_2 in (III.8) is zero at one half turn if $\alpha=0^\circ$ or $\tau=0$, thus yielding two zero frequencies from Love's frequency equation (III.8).

Except for very long springs, it should be noted that the coupling of the spring is increased as α is increased. This coupling in effect separates the two frequencies. For example, consider a spring with $a/\ell = 0.01$

and $R/a = 20$ as shown in figures (III.2a, c). For $\alpha=0^\circ$, the in-plane and out-of-plane dimensionless frequencies are 7.4×10^{-4} and 8.1×10^{-4} respectively. For the same length and R/a , the in-plane frequency decreases and the out-of-plane frequency increases as the pitch angle is increased. However, for very long springs, the separation of the two frequencies is reduced.

4. Configuration of the Rod in the Form of a Ring

For the special case when $\tau=0$, the initial configuration of the rod is in the form of a ring. The $[\gamma]$ matrix of (III.1) can then be written

$$[\gamma_{ij}] = \begin{bmatrix} \gamma^* & \gamma^* & 0 & 0 \\ 11 & 12 & & \\ -\gamma^* & \gamma^* & 0 & 0 \\ 12 & 22 & & \\ 0 & 0 & \gamma^* & \gamma^* \\ & & 33 & 34 \\ 0 & 0 & \gamma^* & \gamma^* \\ & & 34 & 44 \end{bmatrix} \quad \dots(\text{III.9})$$

where $\gamma_{ij}^* = \gamma_{ij}$ of (III.1) with $\tau=0$. The displacement variables U_t and U_1 are now uncoupled from the displacement variables U_2 and U_θ . However, the longitudinal motion is coupled with the in-plane transverse motion, and the out-of-plane transverse motion is coupled with the torsional motion of the rod. For $\tau=0$, the four equations are given by

$$\begin{bmatrix} 1 & 0 \\ 0 & 1 \end{bmatrix} \begin{Bmatrix} \ddot{U}_t \\ \ddot{U}_1 \end{Bmatrix} = \frac{E}{\rho a^2} \begin{bmatrix} \gamma_{11}^* & \gamma_{12}^* \\ -\gamma_{12}^* & \gamma_{22}^* \end{bmatrix} \begin{Bmatrix} U_t \\ U_1 \end{Bmatrix} \quad \dots(\text{III.10})$$

for in-plane and extensional vibrations,

$$\text{and} \quad \begin{bmatrix} 1 & 0 \\ 0 & 2 \end{bmatrix} \begin{Bmatrix} \ddot{U}_2 \\ \ddot{U}_\theta \end{Bmatrix} = \frac{E}{\rho a^2} \begin{bmatrix} \gamma_{33}^* & \gamma_{34}^* \\ \gamma_{34}^* & \gamma_{44}^* \end{bmatrix} \begin{Bmatrix} U_2 \\ U_\theta \end{Bmatrix} \quad \dots(\text{III.11})$$

for out-of-plane and torsional vibrations.

It should be noted that the $[\gamma]$ matrix for any plane curve will be similar to that shown in (III.9), because the uncoupling of the two sets of displacement variables depends on the fact that $\tau=0$ and not on the assumption that κ is constant. Therefore, the statement on the coupling of the longitudinal and in-plane transverse motions, and also the coupling of the out-of-plane transverse and torsional motions is true for rods in the form of plane curves in general.

Spectrum curves for ring segments are also shown in figures (III.2a, b, c, d). The maximum number of turns for ring segments as shown in figures (III.2a, b, c, d) is unity.

5. Frequencies for One Half Ring

Consider the various modes of free vibration of a half ring segment, supported at both ends such that conditions (III.4b) apply. For one half ring

$$\lambda = \frac{\pi a}{l} = \frac{\pi a}{\pi R} = \kappa$$

Let

$$\begin{Bmatrix} U_t \\ U_1 \\ U_2 \\ U_\theta \end{Bmatrix} = \begin{Bmatrix} \eta_t \sin n\lambda\xi \\ \eta_1 \cos n\lambda\xi \\ \eta_2 \sin n\lambda\xi \\ \eta_\theta \sin n\lambda\xi \end{Bmatrix} \sin \omega t \quad \dots(\text{III.12})$$

where n is the number of half wave lengths in the ring segment.

5.a Extensional Vibration

Considering the in-plane vibration part only and substituting for U_t and U_1 in (III.10) yields

$$\begin{bmatrix} (1+\kappa^2)n^2\lambda^2 - \Omega^2 & -n\lambda\kappa(n^2\lambda^2+1) \\ -n\lambda\kappa(n^2\lambda^2+1) & n^4\lambda^4+\kappa^2-\Omega^2 \end{bmatrix} \begin{Bmatrix} \eta_t \\ \eta_1 \end{Bmatrix} = \begin{Bmatrix} 0 \\ 0 \end{Bmatrix} \quad \dots(\text{III.13})$$

It is assumed that for extensional vibration there is no curvature change along the axis of the rod. This can be expressed mathematically as

$$U_1' = \kappa U_t, \quad \text{or} \quad -n\lambda\eta_1 = \kappa\eta_t$$

Substituting for η_1 in the first equation of (III.12), and noting that $\lambda=\kappa=a/R$ yields

$$\begin{aligned} & \left[\left(1 + \frac{a^2}{R^2} \right) n^2 \left(\frac{a}{R} \right)^2 - \Omega^2 + \frac{a^2}{R^2} \left(n^2 \frac{a^2}{R^2} + 1 \right) \right] \eta_t = 0 \\ \text{or } \Omega^2 & \equiv \frac{\rho a^2}{E} \omega^2 = \frac{a^2}{R^2} \left(2 \frac{a^2}{R^2} + n^2 + 1 \right) \end{aligned}$$

The term $\frac{2a^2}{R^2}$ in the above equation can be neglected since $\frac{2a^2}{R^2} \ll 1$.

$$\text{and } \omega^2 = \frac{E}{\rho R^2} (n^2 + 1) \quad \dots \text{(III.14)}$$

This agrees with the formula given in Flügge's⁷ Handbook.

5.b Torsional Vibration

Considering only torsional vibration, and substituting for U_2 and U_θ in (III.11) yields

$$\begin{bmatrix} \lambda^4 + \frac{2G}{E} \lambda^2 \kappa^2 - \Omega^2 & \lambda^2 \kappa \left(1 + \frac{2G}{E}\right) \\ \lambda^2 \kappa \left(1 + \frac{2G}{E}\right) & \frac{2G}{E} \lambda^2 + \kappa^2 - 2\Omega^2 \end{bmatrix} \begin{Bmatrix} \eta_2 \\ \eta_\theta \end{Bmatrix} = \begin{Bmatrix} 0 \\ 0 \end{Bmatrix} \quad \dots \text{(III.15)}$$

The second equation of (III.15) becomes

$$n^2 \frac{a^3}{R^3} \left(1 + \frac{2G}{E}\right) \eta_2 + \left(\frac{2G}{E} n^2 \frac{a^2}{R^2} + \frac{a^2}{R^2} - 2\Omega^2\right) \eta_\theta = 0$$

For torsional mode of vibration $\eta_2 \ll \eta_\theta$. In addition, the coefficient of η_2 is of order $\left(\frac{a}{R}\right)^3$, while the coefficient of η_θ is of order $\left(\frac{a}{R}\right)^2$. Since $\left(\frac{a}{R}\right)$ is considered much less than unity, the coefficient of η_2 is of higher order than the coefficient of η_θ . The term

$$n^2 \frac{a^3}{R^3} \left(1 + \frac{2G}{E}\right) \eta_2$$

can therefore be neglected since it is a product of higher order terms, $\left(\frac{a}{R}\right)^3$ and η_2 . Based on this consideration, the equation reduces to

$$\Omega^2 \equiv \frac{\rho a^2}{E} \omega^2 = \frac{a^2}{R^2} \left(n^2 \frac{G}{E} + \frac{1}{2}\right)$$

$$\text{and } \omega^2 = (n^2 + \frac{E}{2G}) \frac{G}{\rho R^2} = (n^2 + 1 + \nu) \frac{G}{\rho R^2} \quad \dots(\text{III.16})$$

This agrees with the formula given in Flügge's⁷ Handbook.

5.c. In-plane Flexural Vibrations

Considering only in-plane flexural motion, and rewriting equations (III.10) in full leads to

$$\left. \begin{aligned} \frac{\rho a^2}{E} \ddot{U}_t &= (1 + \kappa^2) D_2 U_t + \kappa (D_3 - D) U_1 \\ \frac{\rho a^2}{E} \ddot{U}_1 &= \kappa (D - D_3) U_t - (D_4 + \kappa^2) U_1 \end{aligned} \right\} \quad \dots(\text{III.17})$$

Differentiate the first of (III.17) and multiply the result by κ . Also differentiate the second of (III.17) twice. This leads to

$$\kappa \frac{\rho a^2}{E} \ddot{U}'_t = (\kappa + \kappa^3) D_3 U_t + \kappa^2 (D_4 - D_2) U_1 \quad \dots(\text{III.18})$$

$$\frac{\rho a^2}{E} \ddot{U}'_1 = \kappa (D_3 - D_5) U_t - (D_6 + \kappa^2 D_2) U_1 \quad \dots(\text{III.19})$$

Subtracting (III.18) from (III.19) yields

$$\frac{\rho a^2}{E} (\ddot{U}'_1 - \kappa \ddot{U}'_t) = -(\kappa D_4 + \kappa^3 D_2) U_t - (D_6 + \kappa^2 D_4) U_1 \quad \dots(\text{III.20})$$

It is now assumed that for this type of vibration, the axial strain at the center line of the rod is zero, or

$$U'_t = \kappa U_1$$

Equation (III.20) then reduces to

$$\frac{\rho a^2}{E} (\ddot{U}'_1 - \kappa^2 \ddot{U}_1) = (-D_6 - 2\kappa^2 D_4 - \kappa^3 D_2) U_1$$

Substituting for U_1 from (III.12) yields

$$\begin{aligned} \frac{\rho a^2}{E} \omega^2 (n^2 \lambda^2 + \kappa^2) \eta_1 &= (n^6 \lambda^6 - 2\kappa^2 n^4 \lambda^4 + \kappa^3 n^2 \lambda^2) \eta_1 \\ \text{or } \frac{\rho a^2}{E} \omega^2 (n^2 + 1) &= n^2 \frac{a^4}{R^4} (n^2 - 1)^2 \\ \text{and } \omega^2 &= \frac{n^2 (n^2 - 1)^2}{n^2 + 1} \frac{E a^2}{\rho R^4} \quad \dots \text{(III.21)} \end{aligned}$$

This agrees with the formulae given by Love¹ and Flügge⁷.

5.d Out-of-Plane Flexural Vibrations

Considering only out-of-plane flexural motion and assuming that the torsional inertia term can be neglected, i.e.,

$$I_p \ddot{U}_\theta = 0$$

Equations (III.11) then become

$$\begin{aligned} \frac{\rho a^2}{E} \ddot{U}_2 &= \left(\frac{2G}{E} \kappa^2 D_2 - D_4 \right) U_2 + \kappa \left(1 + \frac{2G}{E} \right) D_2 U_\theta \\ &\dots \text{(III.22)} \\ 0 &= \kappa \left(1 + \frac{2G}{E} \right) D_2 U_2 + \left(\frac{2G}{E} D_2 - \kappa^2 \right) U_\theta \end{aligned}$$

Substituting for U_2 and U_θ as given by (III.12) into (III.22) yields

$$\begin{aligned} \left(n^4 \lambda^4 + \frac{2G}{E} n^2 \lambda^2 \kappa^2 - \Omega^2 \right) \eta_2 + \kappa \left(1 + \frac{2G}{E} \right) n^2 \lambda^2 \eta_\theta &= 0 \\ &\dots \text{(III.23)} \\ \kappa \left(1 + \frac{2G}{E} \right) n^2 \lambda^2 \eta_2 + \left(\frac{2G}{E} n^2 \lambda^2 + \kappa^2 \right) \eta_\theta &= 0 \end{aligned}$$

Eliminating η_θ from (III.23) yields

$$\left(n^6 \lambda^6 - n^2 \lambda^2 \Omega^2 + n^2 \lambda^2 \kappa^4 - \frac{\kappa^2 E}{2G} \Omega^2 - 2n^4 \lambda^4 \kappa^2 \right) n_2 = 0$$

$$\text{or } \Omega^2 \left(\frac{E}{2G} \kappa^2 + n^2 \lambda^2 \right) = n^2 \lambda^2 (n^4 \lambda^4 + \kappa^4 - 2n^2 \lambda^2 \kappa^2)$$

$$\text{and } \omega^2 = \frac{n^2 (n^2 - 1)^2 E a^2}{(n^2 + 1 + \nu) \rho R^4} \dots (\text{III.24})$$

where ν is Poisson's ratio and is given by $1 + \nu = \frac{E}{2G}$.

(III.24) agrees with the formulae given by Love¹ and Flügge⁷.

Equations (III.14), (III.16), (III.21) and (III.24) will now be used to check the frequencies obtained in Table III.1 for the one half ring case.

With $n=1$, $E=30 \times 10^6$ psi, $G=12 \times 10^6$ psi,
 $\rho=0.734 \times 10^{-3}$ lb sec²/in⁴, $R=1.52$ ", $d=0.266$ "

$$\text{(III.14) yields } \omega^2 = \frac{2E}{\rho R^2} = 3.56 \times 10^{10}$$

$$\text{and } \omega = \sqrt{3.56 \times 10^{10}} / 2\pi \doteq 30,000 \text{ cps.}$$

$$\text{(III.16) yields } \omega^2 = \frac{2.25G}{\rho R^2} = 1.60 \times 10^{10}$$

$$\text{and } \omega = \sqrt{1.60 \times 10^{10}} / 2\pi \doteq 20,160 \text{ cps.}$$

(III.21) and (III.24) yield $\omega=0$.

These values for the extensional, torsional and the two flexural frequencies agree with the values in Table III.1.

6. Configuration in a Straight Rod

Here $\tau=\kappa=0$, and (III.5) becomes

$$\begin{bmatrix} \lambda^2 - \Omega^2 & 0 & 0 & 0 \\ 0 & \lambda^4 - \Omega^2 & 0 & 0 \\ 0 & 0 & \lambda^4 - \Omega^2 & 0 \\ 0 & 0 & 0 & \frac{2G}{E}\lambda^2 - 2\Omega^2 \end{bmatrix} \begin{Bmatrix} n_1 \\ n_1 \\ n_2 \\ n_\theta \end{Bmatrix} = \begin{Bmatrix} 0 \\ 0 \\ 0 \\ 0 \end{Bmatrix}$$

... (III.25)

For a straight rod, the $[\gamma]$ matrix becomes a diagonal matrix and all four forms of motions are uncoupled. It can be recognized that in this case, the first and fourth scalar equations of (III.25) represent the longitudinal and torsional motions for a straight rod as given in many books on vibrations⁸. Also the second and third scalar equations of (III.25) can be recognized as the Euler-Bernouilli beam equations for the flexural vibrations of a straight beam.

7. Accuracy of Love's Frequencies

The frequencies obtained from Love's frequency equation (III.8) can be compared with the flexural frequencies obtained after solving (III.5). Table III.2 shows that for "long" springs and springs of small pitch angle, the frequencies given by (III.8) and (III.5) are essentially the same.

Love's frequency equation (III.8) therefore gives good results, and the assumptions made in its development are valid.

For most practical purposes, only the lowest natural frequencies are of interest. In this case, Love's

equation provides a simple way to determine the natural frequencies. However, for short springs and springs with large curvature, equations (III.5) should be used to obtain the natural frequencies.

TABLE III.2

Spring Data: $d = 0.266$ " : $\rho = 0.734 \times 10^{-3}$ lb-sec²/in⁴
 $E = 30 \times 10^6$ psi : $G = 12 \times 10^6$ psi.

α°	R/a	No. of Turns	Love's			
			Frequencies (III.5)		Frequencies (III.8)	
			$\Omega_1 \times 10^{-2}$	$\Omega_2 \times 10^{-2}$	$\Omega_{1L} \times 10^{-2}$	$\Omega_{2L} \times 10^{-2}$
5	15	0.1	9.822	10.56	9.994	10.73
	20		5.573	5.984	5.622	6.037
	25		3.579	3.843	3.598	3.864
15	15		8.661	10.64	8.772	10.84
	20		4.901	6.040	4.934	6.096
	25		3.145	3.879	3.158	3.901
30	15		6.375	9.515	6.417	9.648
	20		3.597	5.389	3.610	5.427
	25		2.305	3.458	2.310	3.473
5	15	0.7	0.1028	0.1423	0.1030	0.1426
	20		0.0579	0.0801	0.0579	0.0802
	25		0.0371	0.0513	0.0371	0.0513
15	15		0.0731	0.1845	0.0731	0.1850
	20		0.0411	0.1039	0.0411	0.1040
	25		0.0263	0.0665	0.0263	0.0666
30	15		0.0423	0.2375	0.0423	0.2381
	20		0.0238	0.1336	0.0238	0.1339
	25		0.0152	0.0856	0.0152	0.0857
5	15	5.0	0.0390	0.0436	0.0390	0.0436
	20		0.0220	0.0254	0.0220	0.0254
	25		0.0141	0.0157	0.0141	0.0157
15	15		0.0377	0.0424	0.0377	0.0424
	20		0.0212	0.0239	0.0212	0.0239
	25		0.0136	0.0153	0.0136	0.0153
30	15		0.0335	0.0382	0.0335	0.0382
	20		0.0189	0.0215	0.0189	0.0215
	25		0.0121	0.0138	0.0121	0.0138

CHAPTER IV

GENERAL SOLUTION FOR HELICAL SPRING PROBLEM

1. Introduction

In the previous chapter, dealing with the investigation of wave propagation in a Helical Spring, it was shown that Love's approximations were valid for most springs. For simplicity, therefore, these approximations will be used in this development to formulate a general solution for the helical spring problem subjected to different boundary conditions in this chapter.

Love's approximations are

(i) Neglect torsional inertia or $I_p \ddot{U} = 0$

(ii) Assume that the axial strain at the rod centerline is zero, or $U'_t = \kappa U_1$

By neglecting the applied loading terms, equations (II.18), (II.21), (II.22) and (II.23) can be written

$$\rho I_a \ddot{U}_t = a N'_t + \kappa \tau M_1 + \kappa M'_2 \quad \dots (IV.1)$$

$$\rho I_a \ddot{U}_1 = a \kappa N_t - \kappa \tau M_t - 2\tau M'_1 + \tau^2 M_2 - M'_2 \quad \dots (IV.2)$$

$$\rho I_a \ddot{U}_2 = \kappa M'_t + M'_1 - \tau^2 M_2 - 2\tau M'_2 \quad \dots (IV.3)$$

$$0 = M'_t - \kappa M_1 \quad \dots (IV.4)$$

By eliminating the axial force N_t from (IV.1) and (IV.2) and differentiating the result once with respect to ξ yields

$$\rho I_a [\ddot{U}_1' - \kappa \ddot{U}_t'] = \tau^2 M_2'' - \kappa \tau M_t'' - 2\tau M_1''' - M_2'''' - \kappa^2 (\tau M_1' + M_2') \quad \dots (IV.5)$$

$$\rho I_a \ddot{U}_2' = \kappa M_t'' + M_1''' - \tau^2 M_1'' - 2\tau M_2' \quad \dots (IV.6)$$

$$0 = M_t'' - \kappa M_1' \quad \dots (IV.7)$$

Substituting for M_t , M_1 and M_2 from equations (II.24) to (II.26) into the three equations above, and using the inextensibility of the centerline assumption, $U_t' = \kappa U_1$ on the resulting three equations yields

$$\begin{aligned} \frac{\rho a^2}{E} [\ddot{U}_1' - \kappa^2 \ddot{U}_1] &= \left[-D_6 + (6\tau^2 - 2\kappa^2) D_4 + (\kappa^2 \tau^2 (6-m) - \tau^4 - \kappa^4) D_2 + \kappa^4 \tau^2 \right] U_1 \\ &+ \left[4\tau D_5 + (\kappa^2 \tau (3-m) - 4\tau^3) D_3 - (\kappa^2 \tau^3) D \right] U_2 \\ &+ \left[\kappa \tau (-2-m) D_3 - \kappa^3 \tau D \right] U_\theta \quad \dots (IV.8) \end{aligned}$$

$$\begin{aligned} \frac{\rho a^2}{E} \ddot{U}_2' &= \left[-4\tau D_4 + (4\tau^3 + \kappa^2 \tau (m-3)) D_2 + \tau^3 \kappa^2 \right] U_1 \\ &+ \left[-D_5 + (6\tau^2 + m\kappa^2) D_3 - \tau^4 D \right] U_2 \\ &+ \left[\kappa (1+m) D_3 - \tau^2 \kappa D \right] U_\theta \quad \dots (IV.9) \end{aligned}$$

$$\begin{aligned} 0 &= \left[\kappa \tau (2+m) D_2 + \tau \kappa^3 \right] U_1 \\ &+ \left[\kappa (1+m) D_3 - \kappa \tau^2 D \right] U_2 + \left[m D_3 - \kappa^2 D \right] U_\theta \quad \dots (IV.10) \end{aligned}$$

where $m \equiv 2G/E$

$$\begin{aligned} \text{Letting } U_1 &= \Delta_1(\xi) e^{i\omega t} \\ U_2 &= \Delta_2(\xi) e^{i\omega t} \\ U_\theta &= \Delta_\theta(\xi) e^{i\omega t} \end{aligned}$$

yields upon substitution into (IV.8) to (IV.10) the following systems of equations in matrix form.

$$\begin{bmatrix} -D_6 + a_1 D_4 + a_2 D_2 + a_3 & a_4 D_5 + a_5 D_3 + a_6 D & a_7 D_3 + a_8 D \\ -a_4 D_4 - a_5 D_2 - a_6 & -D_5 + a_9 D_3 + a_{10} D & a_{11} D_3 + a_{12} D \\ -a_7 D_2 - a_8 & a_{11} D_3 + a_{12} D & a_{13} D_3 + a_{14} D \end{bmatrix} \begin{Bmatrix} \Delta_1(\xi) \\ \Delta_2(\xi) \\ \Delta_\theta(\xi) \end{Bmatrix} = \begin{Bmatrix} 0 \\ 0 \\ 0 \end{Bmatrix}$$

... (IV.11)

where

$$\begin{aligned} a_1 &= 6\tau^2 - 2\kappa^2 \\ a_2 &= \kappa^2 \tau^2 (6-m) - \tau^4 - \kappa^4 + \Omega^2 \\ a_3 &= \kappa^4 \tau^2 - \kappa^2 \Omega^2 \\ a_4 &= 4\tau \\ a_5 &= \kappa^2 \tau (3-m) - 4\tau^3 \\ a_6 &= -\kappa^2 \tau^3 \\ a_7 &= \kappa \tau (-2-m) \\ a_8 &= -\kappa^3 \tau \\ a_9 &= 6\tau^2 + m\kappa^2 \\ a_{10} &= \Omega^2 - \tau^4 \\ a_{11} &= \kappa(1+m) \\ a_{12} &= -\tau^2 \kappa \\ a_{13} &= m \\ a_{14} &= -\kappa^2 \quad \text{and} \quad \Omega^2 = \frac{\rho a^2 \omega^2}{E} \end{aligned}$$

Equations (IV.11) are a set of coupled ordinary differential equations with constant coefficients.

Assuming a solution of the form

$$\Delta_1(\xi) = \alpha e^{\mu\xi}$$

$$\Delta_2(\xi) = \beta e^{\mu\xi}$$

$$\Delta_\theta(\xi) = \gamma e^{\mu\xi}$$

and substituting into (IV.11) yields

$$\begin{bmatrix} -\mu^6 + a_1\mu^4 + a_2\mu^2 + a_3 & a_4\mu^5 + a_5\mu^3 + a_6\mu & a_7\mu^3 + a_8\mu \\ -a_4\mu^4 - a_5\mu^2 - a_6 & -\mu^5 + a_9\mu^3 + a_{10}\mu & a_{11}\mu^3 + a_{12}\mu \\ -a_7\mu^2 - a_8 & a_{11}\mu^3 + a_{12}\mu & a_{13}\mu^3 + a_{14}\mu \end{bmatrix} \begin{Bmatrix} \alpha \\ \beta \\ \gamma \end{Bmatrix} = \begin{Bmatrix} 0 \\ 0 \\ 0 \end{Bmatrix}$$

... (IV.12)

Eliminating γ from (IV.12) yields

$$\begin{bmatrix} b_1\mu^8 + b_2\mu^6 + b_3\mu^4 + b_4\mu^2 + b_5 & b_6\mu^7 + b_7\mu^5 + b_8\mu^3 \\ -b_6\mu^5 - b_7\mu^3 - b_8\mu & b_1\mu^6 + b_9\mu^4 + b_{10}\mu^2 + b_{11} \end{bmatrix} \begin{Bmatrix} \alpha \\ \beta \end{Bmatrix} = \begin{Bmatrix} 0 \\ 0 \end{Bmatrix}$$

... (IV.13)

where $b_1 = -m$

$$b_2 = 6m\tau^2 + \kappa^2(1-2m)$$

$$b_3 = \kappa^2\tau^2(10m-2) + \kappa^4(2-m) + m(\Omega^2 - \tau^4)$$

$$b_4 = \kappa^4\tau^2(4m-2) + \kappa^6 + \tau^4\kappa^2 - \kappa^2\Omega^2(1+m)$$

$$b_5 = \kappa^4\Omega^2$$

$$b_6 = 4m\tau$$

$$b_7 = \kappa^2\tau(6m-2) - 4m\tau^2$$

$$b_8 = 2(1-m)(\kappa^2\tau^3 - \kappa^4\tau)$$

$$b_9 = 2m(3\tau^2 - \kappa^2)$$

$$b_{10} = \kappa^2 \tau^2 (2m-4) + m(\Omega^2 - \kappa^4 - \tau^4)$$

$$b_{11} = -\kappa^2 \Omega^2$$

For nontrivial values of α and β in (IV.13), it is required that the determinant of the coefficients of α and β in (IV.13) be zero.

This leads to the characteristic equation upon expansion

$$\mu^2 \left[m\mu^{12} + C_1\mu^{10} + C_2\mu^8 + C_3\mu^6 + C_4\mu^4 + C_5\mu^2 + C_6 \right] = 0 \quad \dots(\text{IV.14})$$

There are two zero roots of (IV.14), corresponding to rigid body motion. These will be neglected from the characteristic equation, since only vibratory motions are of interest.

In (IV.14), the coefficients C_i , ($i = 1, 2, \dots, 6$) are defined as

$$C_1 = 4m(\kappa^2 + \tau^2)$$

$$C_2 = m \left[6(2\kappa^2\tau^2 + \kappa^4 + \tau^4) - 2\Omega^2 \right]$$

$$C_3 = 4m(\tau^6 + 3\kappa^4\tau^2 + 3\tau^4\kappa^2 + \kappa^6) + \Omega^2 \left[\kappa^2(1-3m) + 12m\tau^2 \right]$$

$$C_4 = m \left[\tau^8 + \kappa^8 + 4(\tau^6\kappa^2 + \kappa^6\tau^2 + 1.5\kappa^4\tau^4) \right] + \Omega^2 \left[2\kappa^4 + \tau^2\kappa^2(6m-6) - 2m\tau^4 + m\Omega^2 \right]$$

$$C_5 = \Omega^2\kappa^2(m+1) \left[2\tau^2\kappa^2 + \kappa^4 + \tau^4 - \Omega^2 \right]$$

$$C_6 = \kappa^4\Omega^4$$

Neglecting the zero roots the characteristic equation can be written

$$m\eta^6 + C_1\eta^5 + C_2\eta^4 + C_3\eta^3 + C_4\eta^2 + C_5\eta + C_6 = 0 \quad \dots(\text{IV.15})$$

where $n=\mu^2$, in order to reduce the degree of the polynomial.

In general, the twelve roots μ_i , ($i=1, 2, \dots, 12$) of the characteristic equation for a given non-zero frequency may be real, imaginary or complex. Depending on the nature of the roots the solutions for $\Delta_1(\xi)$, $\Delta_2(\xi)$ and $\Delta_\theta(\xi)$ result in different forms. After getting the roots μ_i , ($i=1, 2, \dots, 12$), the solutions can be written in the form

$$\begin{aligned}\Delta_1(\xi) &= \sum_{j=1}^{12} \alpha_j e^{\mu_j \xi} \\ \Delta_2(\xi) &= \sum_{j=1}^{12} \beta_j e^{\mu_j \xi} \\ \Delta_\theta(\xi) &= \sum_{j=1}^{12} \gamma_j e^{\mu_j \xi}\end{aligned} \quad \dots(\text{IV.16})$$

where α_j , β_j and γ_j , ($j=1, 2, \dots, 12$) are related by equation (IV.17)

$$\left. \begin{aligned}\alpha_j &= 1 \\ \beta_j &= \frac{b_8 \mu_j + b_7 \mu_j^3 + b_6 \mu_j^5}{b_{11} + b_{10} \mu_j^2 + b_9 \mu_j^4 + b_1 \mu_j^6} \\ \gamma_j &= \frac{a_8 - a_{12} \beta_j \mu_j + a_7 \mu_j^2 - a_{11} \beta_j \mu_j^3}{a_{14} \mu_j + a_{13} \mu_j^3}\end{aligned} \right\} \dots(\text{IV.17})$$

Equations (IV.17) are obtained by arbitrarily setting $\alpha_j=1$ and by solving for β_j and γ_j from (IV.13) and (IV.12) respectively, for each of the twelve roots obtained.

2. Nature of the Roots of the Characteristic Equation

A negative root η yields two imaginary roots μ_j and μ_{j+1} , one being the conjugate of the other. β_j and β_{j+1} will be imaginary, and will occur in complex pairs after substitution of μ_j and μ_{j+1} in (IV.17). A similar condition exists for γ_j and γ_{j+1} . Let the imaginary parts of β_j and γ_j be X_j and \bar{X}_j respectively. Then the part of the general solution (IV.16) contributed by μ_j and μ_{j+1} can be written

$$\begin{aligned}\Delta_1(\xi) &= K_j \text{Sin } s_j \xi + K_{j+1} \text{Cos } s_j \xi \\ \Delta_2(\xi) &= X_j (K_j \text{Cos } s_j \xi - K_{j+1} \text{Sin } s_j \xi) \quad \dots \text{(IV.18)} \\ \Delta_3(\xi) &= \bar{X}_j (K_j \text{Cos } s_j \xi - K_{j+1} \text{Sin } s_j \xi)\end{aligned}$$

where s_j is the imaginary part of μ_j .

Similarly, a complex root η yields two complex roots μ_j and μ_{j+1} , one being the conjugate of the other. β_j and β_{j+1} will be complex, occurring in complex conjugate pairs. Similarly, γ_j and γ_{j+1} will be complex conjugate pairs. Let the real parts of β_j and γ_j be W_j and \bar{W}_j respectively. Let the imaginary parts of β_j and γ_j be Z_j and \bar{Z}_j respectively. Then the part of the general solution (IV.16) contributed by the pair of complex roots μ_j and μ_{j+1} is

$$\begin{aligned}\Delta_1(\xi) &= e^{r_j \xi} (K_j \text{Sin } s_j \xi + K_{j+1} \text{Cos } s_j \xi) \\ \Delta_2(\xi) &= e^{r_j \xi} \left[K_j (Z_j \text{Cos } s_j \xi + W_j \text{Sin } s_j \xi) + K_{j+1} (W_j \text{Cos } s_j \xi \right. \\ &\quad \left. - Z_j \text{Sin } s_j \xi) \right] \quad \dots \text{(IV.19)}\end{aligned}$$

$$\Delta_{\theta}(\xi) = e^{r_j \xi} \left[K_j (\bar{Z}_j \cos s_j \xi + \bar{W}_j \sin s_j \xi) + K_{j+1} (\bar{W}_j \cos s_j \xi - \bar{Z}_j \sin s_j \xi) \right]$$

where r_j is the real part of μ_j

and s_j is the imaginary part of μ_j .

For the third possibility, a real and positive root n yields two real roots μ_j and μ_{j+1} , one being the negative of the other. β_j and β_{j+1} will be real, one being the negative of the other. Also, γ_j and γ_{j+1} will be real. Let the real parts of β_j and γ_j be Y and \bar{Y} respectively in this case. Then the part of the general solution (IV.16) contributed by the pair of real roots μ_j and μ_{j+1} can be written

$$\Delta_1(\xi) = K_j \sinh r_j \xi + K_{j+1} \cosh r_j \xi$$

$$\Delta_2(\xi) = Y(K_j \cosh r_j \xi + K_{j+1} \sinh r_j \xi) \quad \dots (IV.20)$$

$$\Delta_{\theta}(\xi) = \bar{Y}(K_j \cosh r_j \xi + K_{j+1} \sinh r_j \xi)$$

where r_j is the real part of μ_j .

For each $\Delta_1(\xi)$, as given by (IV.18), (IV.19) and (IV.20), depending on the nature of μ_j and μ_{j+1} , Love's approximation $\Delta'_t = K\Delta_1$ can be used to obtain the corresponding part of the general solution for $\Delta_t(\xi)$.

3. Example

Consider a hypothetical case where $\mu_1, \mu_2, \mu_3, \mu_4, \mu_5$, and μ_6 are imaginary, μ_7, μ_8, μ_9 and μ_{10} are complex, and μ_{11}, μ_{12} are real, the relationships between μ_j and

μ_{j+1} , ($j=1, 3, 5, \dots, 11$) as outlined in the previous section.

Then the complete general solutions for $\Delta_t(\xi)$, $\Delta_1(\xi)$, $\Delta_2(\xi)$ and $\Delta_\theta(\xi)$ can be written

$$\begin{aligned} \Delta_t(\xi) = & \frac{\kappa}{s_1} (-K_1 \cos x_1 + K_2 \sin x_1) + \frac{\kappa}{s_3} (-K_3 \cos x_3 + K_4 \sin x_3) \\ & + \frac{\kappa}{s_5} (-K_5 \cos x_5 + K_6 \sin x_5) \\ & + \frac{\kappa e^{\frac{r_7 \xi}{2}}}{r_7^2 + s_7^2} \left[K_7 (r_7 \sin x_7 - s_7 \cos x_7) + K_8 (r_7 \cos x_7 + s_7 \sin x_7) \right] \\ & + \frac{\kappa e^{\frac{r_9 \xi}{2}}}{r_9^2 + s_9^2} \left[K_9 (r_9 \sin x_9 - s_9 \cos x_9) + K_{10} (r_9 \cos x_9 + s_9 \sin x_9) \right] \\ & + \frac{\kappa}{r_{11}} \left[K_{11} \cosh (r_{11} \xi) + K_{12} \sinh (r_{11} \xi) \right] \quad \dots \text{(IV.21)} \end{aligned}$$

$$\begin{aligned} \Delta_1(\xi) = & K_1 \sin x_1 + K_2 \cos x_1 + K_3 \sin x_3 + K_4 \cos x_3 + K_5 \sin x_5 + K_6 \cos x_5 \\ & + e^{\frac{r_7 \xi}{2}} (K_7 \sin x_7 + K_8 \cos x_7) + e^{\frac{r_9 \xi}{2}} (K_9 \sin x_9 + K_{10} \cos x_9) \\ & + K_{11} \sinh (r_{11} \xi) + K_{12} \cosh (r_{11} \xi) \quad \dots \text{(IV.22)} \end{aligned}$$

$$\begin{aligned} \Delta_2(\xi) = & X_1 (K_1 \cos x_1 + K_2 \sin x_1) + X_3 (K_3 \cos x_3 + K_4 \sin x_3) \\ & + X_5 (K_5 \cos x_5 + K_6 \sin x_5) \\ & + e^{\frac{r_7 \xi}{2}} \left[K_7 (Z_7 \cos x_7 + W_7 \sin x_7) + K_8 (W_7 \cos x_7 - Z_7 \sin x_7) \right] \\ & + e^{\frac{r_9 \xi}{2}} \left[K_9 (Z_9 \cos x_9 + W_9 \sin x_9) + K_{10} (W_9 \cos x_9 - Z_9 \sin x_9) \right] \\ & + Y_{11} \left[K_{11} \cosh (r_{11} \xi) + K_{12} \sinh (r_{11} \xi) \right] \quad \dots \text{(IV.23)} \end{aligned}$$

$$\begin{aligned}
\Delta_{\theta}(\xi) = & \bar{X}_1(K_1 \cos x_1 + K_2 \sin x_1) + \bar{X}_3(K_3 \cos x_3 + K_4 \sin x_3) \\
& + \bar{X}_5(K_5 \cos x_5 + K_6 \sin x_5) \\
& + e^{r_7 \xi} \left[K_7(\bar{Z}_7 \cos x_7 + \bar{W}_7 \sin x_7) + K_8(\bar{W}_7 \cos x_7 - \bar{Z}_7 \sin x_7) \right] \\
& + e^{r_9 \xi} \left[K_9(\bar{Z}_9 \cos x_9 + \bar{W}_9 \sin x_9) + K_{10}(\bar{W}_9 \cos x_9 - \bar{Z}_9 \sin x_9) \right] \\
& + \bar{Y}_{11} \left[K_{11} \cosh(r_{11} \xi) + K_{12} \sinh(r_{11} \xi) \right] \quad \dots \text{(IV.24)}
\end{aligned}$$

where $x_i = s_i \xi$, ($i=1, 3, 5, \dots, 11$).

Thus, the solutions of the set of differential equations (IV.11) are given by equations (IV.21) to (IV.24). The twelve arbitrary constants K_i , ($i=1, 2, \dots, 12$) are determined by imposing the proper boundary conditions at both ends of the spring. There are six conditions at each end, and altogether, there are twelve conditions to be satisfied.

In general, it is not possible to satisfy all twelve conditions simultaneously unless the frequency of the oscillations Ω is a natural frequency of the system. If the frequency is one of the natural frequencies, the ratios among the arbitrary constants \check{K}_i can also be determined. To illustrate the procedure, consider a spring with its ends supported so that there is no rotation, no axial displacement and transverse motion in the binormal direction. The boundary conditions can be expressed mathematically as

$$\Delta_t(\xi) = \Delta'_1(\xi) = \Delta_2(\xi) = \Delta''_2(\xi) = \Delta'''_1(\xi) = \Delta_{\theta} = 0 \text{ at } \xi=0 \text{ and } \xi/a \dots \text{(IV.25)}$$

These boundary conditions were considered in chapter III in connection with the harmonic wave propagation study. Imposing the boundary conditions (IV.25) on equations (IV.21) to (IV.24) and evaluating at $\xi=0$ and ℓ/a in turn yields

$$\begin{bmatrix} D_{11} & D_{1,12} \\ D_{12,1} & D_{12,12} \end{bmatrix} \begin{Bmatrix} K_1 \\ K_{12} \end{Bmatrix} = \begin{Bmatrix} 0 \\ \vdots \\ 0 \end{Bmatrix} \quad \dots (IV.26)$$

where $D_{ij} = D_{ij}(\Omega)$, and the D_{ij} elements for this example are shown in Appendix (A.IV).

In shorthand notation (IV.26) can be written as

$$[D] \{K\} = \{0\} \quad \dots (IV.26a)$$

For nontrivial values of $\{K\}$, $[D]$ has to be singular. Thus a natural frequency of the system under these specific boundary conditions is determined by requiring the determinant of $[D]$ to be zero, i.e.,

$$|D| = 0 \quad \dots (IV.27)$$

If (IV.27) is satisfied, then $\{K\}$ can be determined. Substituting the values of $\{K\}$ into equations (IV.21) to (IV.24) yields the general solution $\Delta_t(\xi)$, $\Delta_1(\xi)$, $\Delta_2(\xi)$ and $\Delta_\theta(\xi)$ respectively. The mode shape for that particular frequency is given by the vector function

$$\begin{Bmatrix} \Delta_t(\xi) \\ \Delta_1(\xi) \\ \Delta_2(\xi) \\ \Delta_\theta(\xi) \end{Bmatrix}$$

The simplest way to obtain a natural frequency of the system is to assume an initial value of frequency. From (IV.15), the values of μ_j , ($j=1, 2, \dots, 12$) are then determined. For a given l/a , the [D] matrix can be formed and the determinant of [D] can be evaluated. In general $|D|$ will not be zero. Another value of frequency is then chosen, and the whole procedure is repeated. Since $|D|$ is a continuous function of the frequency parameter Ω , a plot of $|D|$ against Ω can be made, and the values of Ω at which $|D|$ is zero will give a natural frequency of the system. By varying the values of l/a a spectrum plot can be obtained. A Fortran Program was written to carry out the scheme on the IBM 7040 Electronic Digital Computer. In particular, a check was made on the frequencies calculated for a spring supported so that the end conditions satisfy (IV.25).

Table IV.1 shows that the two methods compare favourably in general. Such comparison gives confidence that the computer program is operational. Each trial value of frequency takes approximately 5 seconds of machine time. This includes the forming and solving of the characteristic equation, the forming of the [D] matrix, and the evaluation of the determinant of [D]. Most of this work was done in double precision arithmetic, since the numbers involved in these calculations were relatively small, and it was desirable to retain accuracy throughout the calculations as much as possible.

TABLE IV.1

Spring Data is same as that given in Table III.1

No. of Turns N	Frequencies from Love's equation cps		Frequencies from General Method cps		
6.5	62.73	70.17	62.7	70.2	
6.25	65.19	72.92	71.1	72.9	
6.0	67.85	75.90	67.9	75.9	
5.75	70.74	79.13		79.1	81.9
5.50	73.88	82.65	73.9	82.7	
5.25	77.30	86.48	77.3	83.3	86.5
5.0	81.05	90.69	81.1	90.7	
4.75	85.17	95.32	85.2		
4.50	89.73	100.43	89.7	100.4	
4.25	94.80	106.12	94.7	106.2	
4.0	100.45	112.47	100.5	112.5	
3.75	106.79	119.60	106.8	119.6	
3.5	113.96	127.67	95.8	113.9	127.7
3.25	122.11	136.87	122.1	136.9	
3.0	131.44	147.42	131.4	147.4	

CHAPTER V
EXPERIMENTAL PROGRAM

1. Introduction

In the previous chapter, it was shown that Love's theory and the General Theory presented gave essentially the same result. In order to provide an indication of the validity of these theories, a series of experiments were performed to find the natural frequencies of a helical spring and to compare them with theoretical values. In the experiment, the spring was held at its ends so that there was no axial displacement, no transverse in-plane motion, no transverse out-of-plane motion and no torsional motion. The ends of the spring were therefore fixed. These boundary conditions can be expressed mathematically as

$$\Delta_t(\xi) = \Delta_1(\xi) = \Delta_2(\xi) = \Delta_\theta(\xi) = \Delta_1'(\xi) = \Delta_2'(\xi) = 0 \text{ at } \xi=0 \text{ and } \ell/a$$

...(V.1)

Two steel springs of varying lengths were tested for these fixed-ended conditions. It was not possible to determine the specific material properties of each spring, i.e., E and G from tests. However, from samples, the mass density of both springs was found to be approximately $0.734 \times 10^{-3} \text{ lb-sec}^2/\text{in}^4$, which is the density of steel.

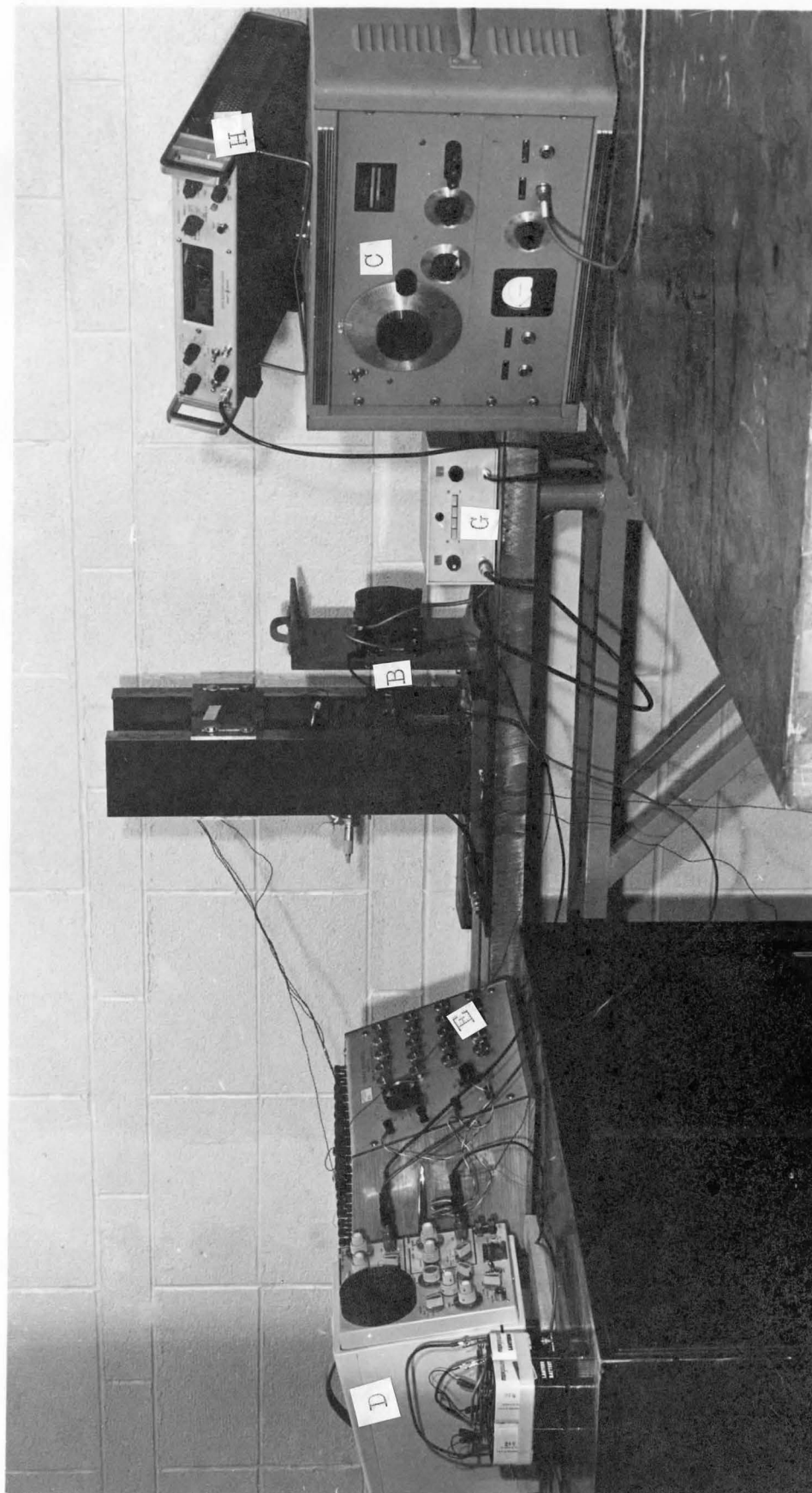


Figure V.1 Experimental Set up.

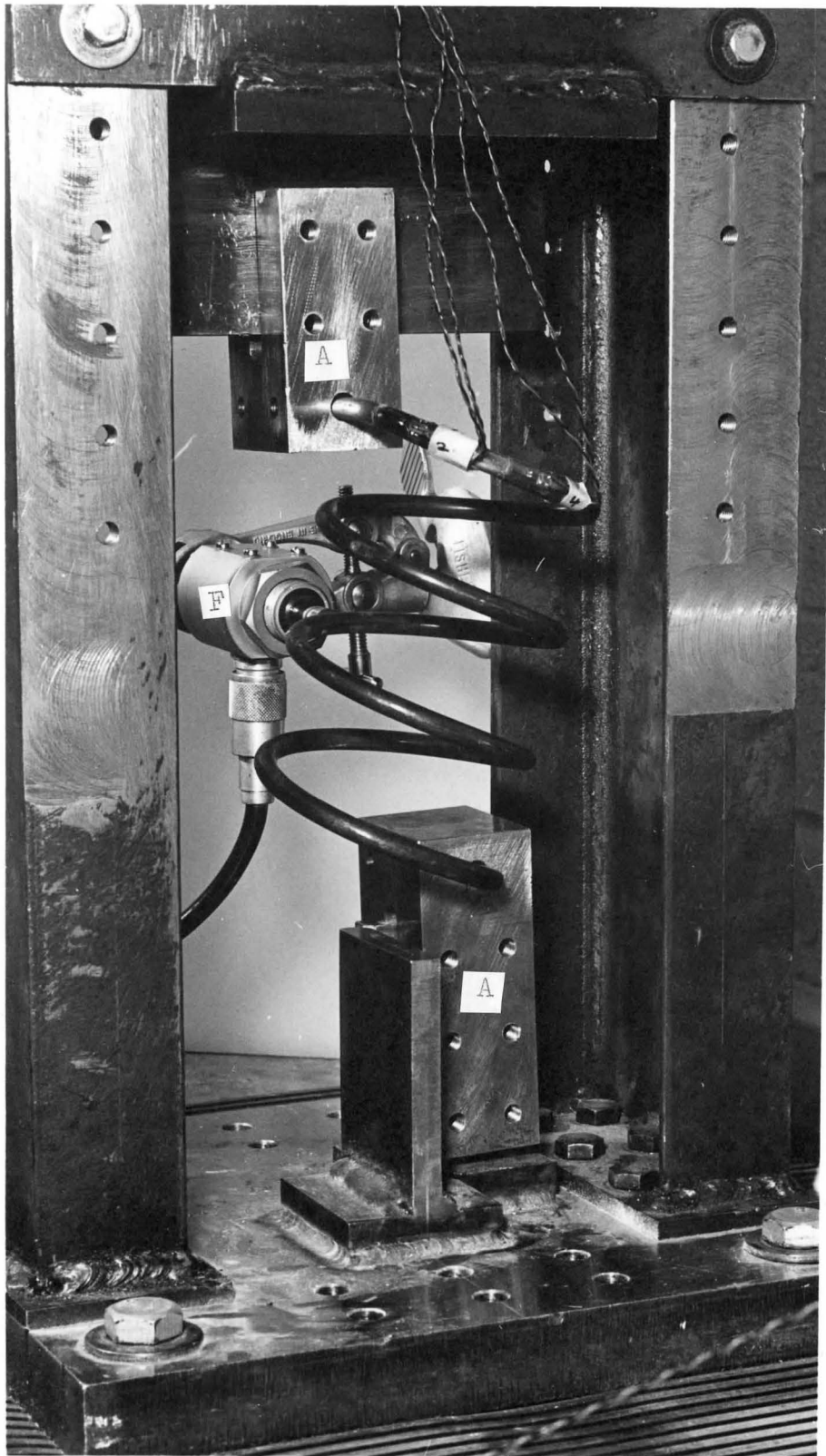


Figure V.2 Test Spring in Position.

The following assumptions for the material properties of the spring were made

$$E = 30 \times 10^6 \text{ psi} : \quad G = 12 \times 10^6 \text{ psi.}$$

Other measured data for the springs were

	d	D	α	Max. No. of Turns
Spring 1	0.266"	3.0"	8.4°	6.5
Spring 2	0.285"	2.9"	7.6°	7.5

2. Experimental Set Up

The general set up of the experiment is shown in figure V.1. The ends of the spring were cut, straightened and levelled so that they would fit into the fixing blocks (A) figure V.11. The blocks were placed at the proper level, so that the entire spring could be slipped into position without having to exert any forces on the spring.

Four strain gauges were mounted near the top of the spring before placing it into position. The legs of the steel table, on which the experiment was performed were bolted to the concrete floor, and vibration pads separated the floor from the bottom of the legs. The frame holding the spring was bolted to the table, with a vibration pad between the bottom plate and the table top.

Figure V.11 shows the bottom plate to which small T-sections were welded, and the top sliding guide to

which larger T-sections were welded. The two fixing blocks (A) can be held securely to the web of the T-sections by screws on both sides of the blocks. With the strain gauges attached, the ends of the spring can be slipped into position, and each end can be held by four more screws. The driver (B) could now be moved into position as shown in figure V.1. The driver arm was attached to the spring at about 1/4 turn from the bottom support, and was held to the spring by means of a pretensioned rubber band.

Four strain gauges (Budd Metalfilm Type C6-121-B-120 ohms \pm .2%) were mounted on the spring. Gauges 1 and 2 were located at about 1/8 turn from the top support. Gauges 3 and 4 were about 1/4 turn from the support. Gauges 1 and 3 were placed so as to measure the out-of-plane bending strain changes, and gauges 2 and 4 were placed to measure the in-plane strain changes.

3. Equipment

An oscillator, (C) figure V.1 (Mod #4100-Electro), frequency range 20-20,000 cps, provided the forcing input to the driver, which in turn excited the spring. Any one of the gauge readings could be obtained on the Parker Bell Dual Beam oscilloscope (D), by switching the leads from the scope to the proper gauge through the switching box (E). The actual frequency of vibration of the spring for any given input could be measured by means of a proximity

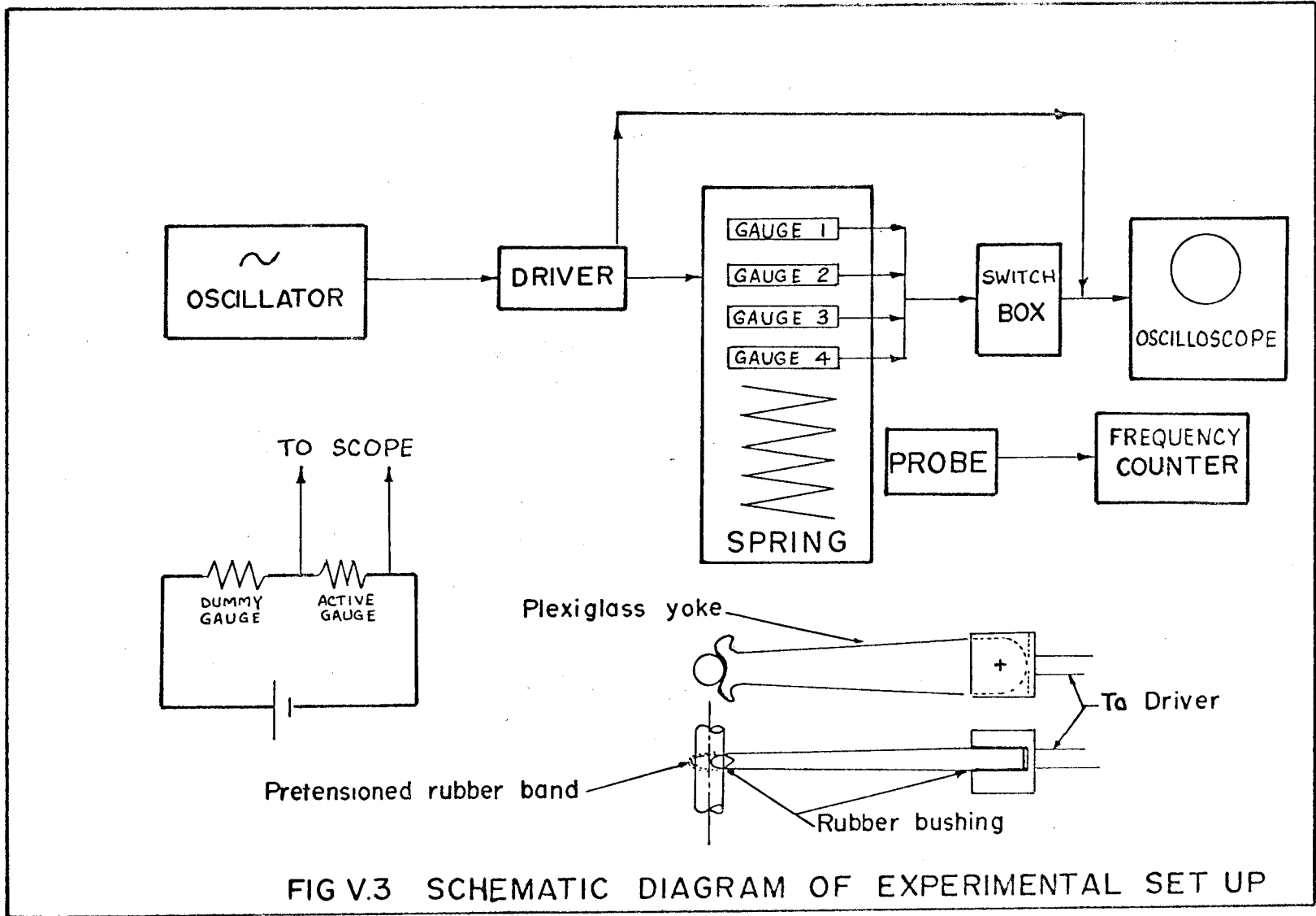


FIG V.3 SCHEMATIC DIAGRAM OF EXPERIMENTAL SET UP

transducer (F) held close to the point at which the frequency of vibration is desired. This was connected to a converter (G), and then to a frequency counter (H) where the frequency was read. A schematic diagram of the experimental set up is shown in figure V.3.

4. Experimental Procedure

With the spring in position, the experiment could be performed after allowing about 30 minutes for the equipment to warm up. The testing procedure was as follows. Starting at the lowest driver frequency, together with a small amplitude setting on the oscillator, the forcing frequency was slowly increased, as the voltages corresponding to the strain measures were read at the scope for all four gauges. The frequency was slowly increased until resonance was observed.

As a natural frequency was approached in this way, one or more of the gauges showed an increase in amplitude on the oscilloscope. At resonance, this amplitude attained a peak value, and large motions of the spring were observed.

At resonance, the following readings are taken: (1) oscillator input frequency; (2) spring output frequency from the electronic counter; (3) driver and all gauge amplitudes. The oscillator amplitude and all range dials on the scope were kept at a constant value throughout the tests, in order to compare the gauge readings.

In addition to measuring the frequencies and gauge readings, an attempt was made to distinguish the mode shape and type of vibration taking place at resonance.

This was done by several methods:

(a) by sight;

(b) by running a small pointed probe along the spring to note the out-of-plane motion and the in-plane motion. As the spring vibrated and touched the small pointed end of the probe, an idea of the predominant type of vibration was obtained;

(c) chalk marks were also placed at certain points along the spring, and the displacement of the chalk particles was used to indicate the type of vibration taking place. The probe was useful in pointing out the node points at higher frequencies. The chalk marks were a bit more useful than the probe in detecting node points because the probe could not easily detect tangential motion of the spring. The chalk marks detected tangential motion more conveniently because of the blurred effect. At resonance there was no blurred effect at the node points.

At or above the second modes of vibration for bending, it became increasingly difficult to measure and note the type of motion taking place at resonance. Because of this, not more than four natural frequencies were found for any length of spring. The procedure was repeated by decreasing the input frequency and repeating all measurements.

5. Comparison of Experimental and Theoretical Results

Following the procedure outlined in chapter IV, a set of equations, similar to (IV.21) to (IV.24) can be developed. The exact form of the equations would depend on the nature of the roots μ_j , ($j=1, 2, \dots, 12$). A $[D_{ij}]$ matrix as in equation (IV.26) can be formed after imposing the boundary conditions of (V.1) on the general solutions obtained. The natural frequencies for this system can be found by assuming a trial value of frequency and requiring that $|D_{ij}(\Omega)|$ be zero. In general $|D_{ij}(\Omega)|$ will not be zero. Another trial value of frequency is assumed and the entire process is repeated. The value of Ω at which $|D_{ij}(\Omega)|$ is zero is a natural frequency of the system. The experimental and theoretical values of natural frequencies are tabulated in Tables V.1 and V.2. The greatest difference between the input and output frequency of vibration was approximately 1%. Only the resonant output frequencies for the first two modes are presented in Tables V.1 and V.2.

6. Discussion of Results

For the two springs tested, the experimental results are in general lower than the theoretical results. Also, the percentage error is smaller for long springs than it is for short springs. The theory predicts the two lowest frequencies within 11% at most.

TABLE V.1 SPRING 1

Spring data: $d = 0.266"$: $D = 3.0"$: $\alpha = 8.4^\circ$
 $E = 30 \times 10^6$ psi: $G = 12 \times 10^6$ psi.

No. of Turns N	No. of Nodes	Experimental freq. ω cps	Theoretical freq. ω cps	% Difference
6.5	0	56.0	63.0	11
	0	70.5	70.6	--
	1	117.0	127.0	8
	1	138.0	139.9	1
5.5	0	73.1	74.0	1
	0	80.4	84.5	5
	1	139.1	141.8	2
	1	149.8	154.5	4
4.5	0	88.0	90.2	2
	0	97.2	103.2	6
	1	105.7	108.2	3
	1	167.2	169.9	2
3.5	0	110.3	114.5	4
	0	122.4	122.4	-
	1	144.5	143.4	-1
	1	191.5	205.7	7
2.5	-	155.1	165.7	6
	-	200.2	208.5	8
	-	241.2	-	-

TABLE V.2 SPRING 2

Spring data: $d = 0.285"$: $D = 2.9"$: $\alpha = 7.5^\circ$ $E = 30 \times 10^6$ psi: $G = 12 \times 10^6$ psi.

No. of Turns N	No. of Nodes	Experimental freq. ω cps	Theoretical freq. ω cps	% Difference
7.5	0	55.8	62.4	9
	0	67.3	71.5	6
	1	117.2	123.0	5
	1	122.4	140.5	13
6.5	0	69.6	72.5	4
	0	76.0	82.5	7
	1	135.9	142.5	5
	1	140.0	152.3	8
5.5	0	80.0	86.8	8
	0	87.2	95.2	8
	1	94.3	100.9	7
	1	153.9	166.7	8
4.5	0	105.7	105.0	1
	0	111.0	112.6	1
	1	178.2	198.1	10
	1	192.0	207.0	7
3.5	0	122.5	134.1	9
	0	135.1	142.3	5
	-	148.7	172.4	14
	-	217.	238.5	9
2.5	-	154.	184.	15
	-	177.	192.	8
	-	193.	246.	22
	-	262.	292.	10

The theory assumes that the spring is stress free prior to testing. This assumption is questionable because of the induced stresses caused by straightening the ends of the spring for testing. Induced stresses due to fabrication may be also present. The fixing blocks could also provide an applied moment at the ends of the spring, thereby creating stresses along the spring. The ends of the spring were assumed to be fixed so that conditions (V.1) apply. There is a possibility that the ends of the spring at resonance could move at the fixing blocks, since a perfectly rigid support is difficult to obtain. This would lower the true frequency of the spring under these end conditions.

The mode shape of the first frequency observed for each spring indicated that in-plane vibration was taking place. Out-of-plane vibration occurred at the second observed frequency. A combination of in-plane and out-of-plane motion was also observed at times. The node points for the higher modes were slightly below the middle of the spring, and were well defined in the longer springs tested. The mode shape and type of vibration were difficult to distinguish as the spring length was reduced. Tables V.1 and V.2 therefore show no information on the number of nodes for springs with 2.5 turns.

CHAPTER VI
CONCLUSIONS AND RECOMMENDATIONS

1. Conclusions

The validity of Love's theory was checked with a more exact theory, and it was shown that Love's theory is good for long springs, and for springs with small curvature in general. However, for short springs and for springs with large curvature, the more exact theory presented in Chapter III should be used to find the natural frequencies for the wave propagation problem in a helical spring.

From a comparison of the experimental and theoretical results for the helical spring with both ends clamped, the following conclusions can be made:

(i) The frequencies obtained from theory compare favourably with those obtained in the experiment, and the theoretical frequencies are in general slightly larger than the experimental frequencies. It can be concluded therefore that the theory can be used to find the natural frequencies for any curved and twisted slender rod, the axis of which is in the form of a general space curve.

(ii) The experimental and theoretical values of frequency both show an expected increase in frequency as the length of the spring decreases.

It was shown in Chapter III that Love's frequencies were higher than the frequencies obtained from the theory presented. The assumptions made for the evaluation of Love's frequencies are in effect added constraints to the system. This would result in frequencies greater than the true frequencies. Similarly, the theory presented in Chapter III did not take into account shear deformation due to bending. A revised theory taking shear deformation into account would be more correct, and the frequencies obtained from this theory would be lower than those shown in Table III.2. As shown in Chapter V, it is not surprising that the experimental frequencies are lower than the theoretical frequencies.

The theory presented can be described as a "Generalised Euler-Bernouilli Beam Theory" for a curved and twisted rod. It was shown in Chapter III that the theory could be reduced to obtain the known natural frequencies for simpler systems, such as rings and straight beams.

2. Recommendations

Quite a lot of work remains to be done on this subject, both analytically and experimentally. The following recommendations are suggested.

(i) The differential equations and the proper boundary conditions should be checked by using the variational method and Hamilton's Principle. This method should give explicitly the natural boundary conditions of the ends of the spring. The differential equations should check with those obtained in Chapter IV. Once these boundary conditions are obtained, analytical results could be obtained for any given end conditions.

(ii) The material properties of the spring should be obtained by experiment or by a curve fitting trial and error procedure.

(iii) More springs should be tested in order to obtain a more general picture of how closely the experimental results agree with the theoretical.

(iv) Although most of the frequency values in Table IV.1, obtained by the General Solution method agree with those obtained from Love's frequency equation, there is some discrepancy. It was only intended to check Love's frequencies, and therefore the initial trial value of frequency was slightly lower than Love's frequency. However, it is noted that for the 3.5 turn spring, the General Solution method predicts a frequency of 95.8 cps., which is an incorrect value. Because the elements of the $[D_{ij}]$ matrix are very small numerically, there is a possibility that rounding errors in the computer operation could result in this incorrect value. K_i , ($i=1, 2, \dots, 12$) could be found for each frequency that makes $|D_{ij}|$ equal

to zero, and hence the mode shape could be obtained. It may be possible to exclude any erroneous frequencies by actually evaluating the mode shape.

(v) A similar study should be done without making Love's approximations for obtaining the natural frequencies of short springs and those with large curvature.

BIBLIOGRAPHY

1. Love, A. E. H., "The Propagation of Waves of Elastic Displacement along a Helical Wire", Cambridge Philosophical Society Trans., Vol.18, 1899, pp. 364-374.
2. Wittrick, W. H., "On Elastic Wave Propagation in Helical Springs", Int. Journal of Mech. Sci., Pergamon Press Ltd., London, England, 1966, Vol.8, pp. 25-47.
3. Ojalvo, I. U., "Coupled Twist-Bending Vibrations of Incomplete Elastic Rings", Int. Journal of Mech. Sci., Pergamon Press Ltd., London, England, 1962, Vol.4, pp.53-72.
4. Massoud, M. P., "Vectorial Derivation of the Equations for Small Vibrations of Twisted Curved Beams", Journal of Applied Mechanics, (June 1965), pp.439-440.
5. Love, A. E. H., "A Treatise on the Mathematical Theory of Elasticity", Dover Publications, New York.
6. Kuo, S. S., "Numerical Methods and Computers", Addison-Wesley Publishing Company, 1966.
7. Flügge, W., "Handbook of Engineering Mechanics", McGraw-Hill Book Company, 1962.
8. Timoshenko, S., "Vibration Problems in Engineering", D. Van Nostrand Company, 1937.

APPENDIX

I. Properties of Helical Spring

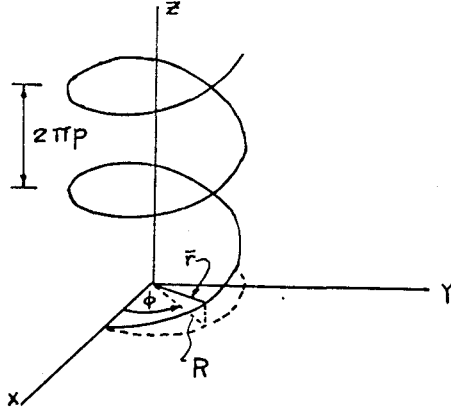


Fig. A.1 - Helical Spring

$$\bar{r} = R \cos \phi \bar{e}_x + R \sin \phi \bar{e}_y + p\phi \bar{e}_z$$

$$\text{and } ds^2 = d\bar{r} \cdot d\bar{r} = d\phi^2 \frac{d\bar{r}}{d\phi} \cdot \frac{d\bar{r}}{d\phi} = (R^2 + p^2) d\phi^2$$

$$\therefore ds = \sqrt{R^2 + p^2} d\phi \text{ and } l = \sqrt{R^2 + p^2} (\phi_1 - \phi_0) \quad \dots (\text{A.I.1})$$

$$\bar{e}_t \equiv \frac{d\bar{r}}{ds} = \frac{d\phi}{ds} \frac{d\bar{r}}{d\phi} = \left(-a \sin \phi \bar{e}_x + a \cos \phi \bar{e}_y + p \bar{e}_z \right) / \sqrt{R^2 + p^2}$$

... (A.I.2)

$$\bar{e}_1 \equiv \frac{d^2 \bar{r}}{ds^2} / \left| \frac{d^2 \bar{r}}{ds^2} \right|, \text{ and } \frac{d^2 \bar{r}}{ds^2} = \frac{d}{ds} \left(\frac{d\bar{r}}{ds} \right) = \frac{d}{ds} \left(\frac{d\phi}{ds} \frac{d\bar{r}}{d\phi} \right)$$

$$= \frac{d}{ds} \frac{d}{d\phi} \left(\frac{d\phi}{ds} \right) \frac{d\bar{r}}{d\phi} + \left(\frac{d\phi}{ds} \right)^2 \frac{d}{d\phi} \frac{d\bar{r}}{d\phi} = \left(\frac{d\phi}{ds} \right)^2 \frac{d^2 \bar{r}}{d\phi^2} \text{ since}$$

$$\frac{d}{d\phi} \left(\frac{d\phi}{ds} \right) = 0$$

$$\therefore \bar{e}_1 = - (\cos \phi \bar{e}_x + \sin \phi \bar{e}_y) \quad \dots (\text{A.I.3})$$

$$\bar{e}_2 = \bar{e}_t \times \bar{e}_1 = (p \sin \phi \bar{e}_x - p \cos \phi \bar{e}_y + R \bar{e}_z) / \sqrt{R^2 + p^2} \quad \dots (A.I.4)$$

$$\kappa_o \equiv \left| \frac{d^2 \bar{r}}{ds^2} \right| = \sqrt{\frac{d^2 \bar{r}}{ds^2} \cdot \frac{d^2 \bar{r}}{ds^2}} = \frac{R}{R^2 + p^2} \quad \dots (A.I.5)$$

$$\tau_o = \frac{1}{\kappa_o} \frac{d\bar{r}}{ds} \cdot \frac{d^2 \bar{r}}{ds^2} \times \frac{d^3 \bar{r}}{ds^3}$$

$$\frac{d^3 \bar{r}}{ds^3} = -R(-\sin \phi \bar{e}_x + \cos \phi \bar{e}_y) / (R^2 + p^2)^{3/2}$$

$$\text{and } \frac{d^2 \bar{r}}{ds^2} \times \frac{d^3 \bar{r}}{ds^3} = R^2 \bar{e}_z / (R^2 + p^2)^{5/2}$$

$$\text{Hence } \tau_o = p / (R^2 + p^2) \quad \dots (A.I.6)$$

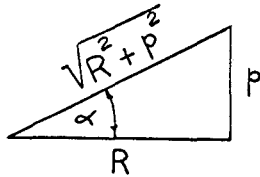
$$\text{Darboux Vector } \bar{D} = \tau_o \bar{e}_t + \kappa_o \bar{e}_2 = \bar{e}_z / (R^2 + p^2) \quad \dots (A.I.7)$$

The vertical projection of the spring in the x-y plane is a circle of radius R. A unit vector along the circumference of this circle is

$$\bar{e} = -\sin \phi \bar{e}_x + \cos \phi \bar{e}_y$$

The pitch angle α is defined by

$$\cos \alpha \equiv \bar{e}_t \cdot \bar{e} = R / \sqrt{R^2 + p^2}$$



$$\therefore \alpha = \tan^{-1} (\text{Pitch}/\pi D) \quad \dots (A.I.8)$$

Radius of gyration for circular section $a = d/4$

$$\text{Now } \kappa_o = R/(R^2 + p^2) = \text{Cos}^2 \alpha / R \text{ and } \kappa \equiv a\kappa_o = \frac{d}{2D} \text{Cos}^2 \alpha \quad \dots (\text{A.I.9})$$

$$\text{also } \tau_o = \kappa_o \text{ Tan } \alpha \text{ and } \tau \equiv a\tau_o = \kappa \text{ Tan } \alpha \quad \dots (\text{A.I.10})$$

The Frenet-Serret Formulae as given in many books on Elasticity are

$$\frac{d\bar{e}_t}{ds} = \kappa_o \bar{e}_1$$

$$\frac{d\bar{e}_1}{ds} = -\kappa_o \bar{e}_t + \tau_o \bar{e}_2 \quad \dots (\text{A.I.11})$$

$$\frac{d\bar{e}_2}{ds} = -\tau_o \bar{e}_1$$

II. Half Turn of Spring

$$\begin{aligned} \text{For half turn, } \lambda &= \frac{\pi a}{l} = \frac{\pi a}{\pi \sqrt{\left(\frac{D}{2}\right)^2 + \left(\frac{D}{2} \text{ Tan } \alpha\right)^2}} \\ &= \frac{d}{2D} \text{Cos } \alpha = \frac{\kappa}{\text{Cos } \alpha} \end{aligned}$$

$$\tau = \kappa \text{ Tan } \alpha$$

$$\therefore C_3 \text{ in (III.8)} = \lambda^4 (\lambda^2 - \kappa^2 - \tau^2)^4 = \lambda^4 (\kappa^2 \text{Sec}^2 \alpha - \kappa^2 - \kappa^2 \text{Tan}^2 \alpha) = 0$$

And (III.8) will yield a zero frequency as long as $\phi = \pi$ in Fig.(A.1), or number of turns = 1/2.

III. Half Turn of Ring

$$\text{For } \tau=0, \lambda = \frac{\pi a}{l} = \frac{\pi a}{\pi R} = \kappa$$

Then C_2 of (III.8) = 0 by inspection, and the fre-

quency equation then yields two zero frequencies.

IV. Elements of D_{ij} - Eq.(IV.26)

The D_{ij} elements of (IV.26) are given by

$$\begin{aligned}
 D_{k,j} &= -\frac{\kappa}{s_j} \text{Cos } s_j \xi & D_{k,j+1} &= \frac{\kappa}{s_j} \text{Sin } s_j \xi \\
 D_{k+1,j} &= s_j \text{Cos } s_j \xi & D_{k+1,j+1} &= -s_j \text{Sin } s_j \xi \\
 D_{k+2,j} &= X_j \text{Cos } s_j \xi & D_{k+2,j+1} &= -X_j \text{Sin } s_j \xi \\
 D_{k+3,j} &= \bar{X}_j \text{Cos } s_j \xi & D_{k+3,j+1} &= -\bar{X}_j \text{Sin } s_j \xi \\
 D_{k+4,j} &= -s_j^2 X_j \text{Cos } s_j \xi & D_{k+4,j+1} &= s_j^2 X_j \text{Sin } s_j \xi \\
 D_{k+5,j} &= -s_j^3 \text{Cos } s_j \xi & D_{k+5,j+1} &= s_j^3 \text{Sin } s_j \xi
 \end{aligned}$$

j=1,3,5

$$D_{k,j} = \frac{r_j e^{r_j \xi}}{r_j^2 + s_j^2} (r_j \text{Sin } s_j \xi - s_j \text{Cos } s_j \xi)$$

$$D_{k+1,j} = e^{r_j \xi} (r_j \text{Sin } s_j \xi + s_j \text{Cos } s_j \xi)$$

$$D_{k+2,j} = e^{r_j \xi} (Z_j \text{Sin } s_j \xi + W_j \text{Cos } s_j \xi)$$

j=7,9

$$D_{k+3,j} = e^{r_j \xi} (\bar{Z}_j \text{Cos } s_j \xi + \bar{W}_j \text{Sin } s_j \xi)$$

$$D_{k+4,j} = e^{r_j \xi} (C_1 \text{Sin } s_j \xi + C_2 \text{Cos } s_j \xi)$$

$$D_{k+5,j} = e^{r_j \xi} (C_3 \text{Sin } s_j \xi + C_4 \text{Cos } s_j \xi)$$

$$D_{k,j+1} = \frac{\kappa e^{r_j \xi}}{r_j^2 + s_j} (r_j \cos s_j \xi + s_j \sin s_j \xi)$$

$$D_{k+1,j+1} = e^{r_j \xi} (r_j \cos s_j \xi - s_j \sin s_j \xi)$$

$$D_{k+2,j+1} = e^{r_j \xi} (W_j \cos s_j \xi - Z_j \sin s_j \xi)$$

j=7,9

$$D_{k+3,j+1} = e^{r_j \xi} (\bar{W}_j \cos s_j \xi - \bar{Z}_j \sin s_j \xi)$$

$$D_{k+4,j+1} = e^{r_j \xi} (C_1 \cos s_j \xi - C_2 \sin s_j \xi)$$

$$D_{k+5,j+1} = e^{r_j \xi} (C_3 \cos s_j \xi - C_4 \sin s_j \xi)$$

$$\text{where } C_1 = W_j (r_j^2 - s_j^2) - 2r_j s_j Z_j$$

$$C_2 = Z_j (r_j^2 - s_j^2) + 2r_j s_j W_j$$

$$C_3 = r_j (r_j^2 - 3s_j^2)$$

$$C_4 = s_j (3r_j^2 - s_j^2)$$

$$D_{k,j} = \frac{\kappa}{r_j} \cosh r_j \xi$$

$$D_{k,j+1} = \frac{\kappa}{r_j} \sinh r_j \xi$$

$$D_{k+1,j} = r_j \cosh r_j \xi$$

$$D_{k+1,j+1} = r_j \sinh r_j \xi$$

$$D_{k+2,j} = Y_j \cosh r_j \xi$$

$$D_{k+2,j+1} = Y_j \sinh r_j \xi$$

j=11

$$D_{k+3,j} = \bar{Y}_j \cosh r_j \xi$$

$$D_{k+3,j+1} = \bar{Y}_j \sinh r_j \xi$$

$$D_{k+4,j} = r_j^2 Y_j \cosh r_j \xi$$

$$D_{k+4,j+1} = r_j^2 Y_j \sinh r_j \xi$$

$$D_{k+5,j} = r_j^3 \cosh r_j \xi$$

$$D_{k+5,j+1} = r_j^3 \sinh r_j \xi$$

With $k=1$ and $\xi=0$ the first six rows of $D_{i,j}$ are filled. With $k=7$ and $\xi=l/a$, the last six rows of the $D_{i,j}$ matrix are filled.

V. Derivation of Generalised Force-Displacement Relationships

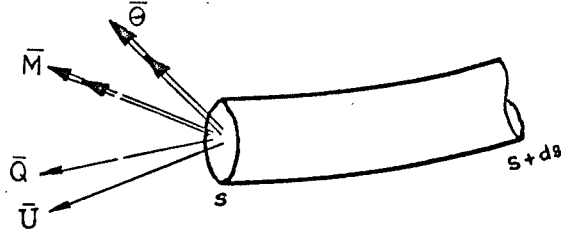


Figure A.2

In fig.(A.2), let $\bar{\theta}$, \bar{U} , \bar{M} and \bar{Q} be vectors representing the resultant rotation, displacement, internal moment and internal force respectively at a cross section s , so that

$$\bar{\theta} = \theta_1 \bar{e}_1 + \theta_2 \bar{e}_2 + \theta_t \bar{e}_t$$

$$\bar{U} = u_1 \bar{e}_1 + u_2 \bar{e}_2 + u_t \bar{e}_t$$

$$\bar{M} = M_1 \bar{e}_1 + M_2 \bar{e}_2 + M_t \bar{e}_t$$

$$\bar{Q} = Q_1 \bar{e}_1 + Q_2 \bar{e}_2 + N_t \bar{e}_t$$

Consider the deformation of element ds . The rotation of the cross-section ($s+ds$) relative to that of the section s is $\left(\frac{\partial \theta}{\partial s}\right) ds$.

∴ By definition of flexural and torsional rigidities:

$$\left(\frac{\partial \theta}{\partial s}\right) ds = \frac{M_t}{\beta_t} \bar{e}_t ds + \frac{M_1}{\beta_1} \bar{e}_1 ds + \frac{M_2}{\beta_2} \bar{e}_2 ds \quad \dots (A.II.1)$$

Also, the displacement of section (s+ds) relative to that of section s is

$$\left(\frac{\partial \bar{U}}{\partial s}\right) ds = \frac{N_t}{\sigma_t} \bar{e}_t ds + \left(\frac{Q_1}{\sigma_1} + \theta_2\right) \bar{e}_1 ds + \left(\frac{Q_2}{\sigma_2} - \theta_1\right) \bar{e}_2 ds$$

... (A.II.2)

where β_t , β_1 and β_2 are the torsional and two flexural rigidities of rod,

σ_t , σ_1 and σ_2 are the extensional and two shear rigidities of the rod.

Cancel ds from (A.II.1) and perform the differentiation to yield

$$\begin{aligned} \frac{\partial \theta_t}{\partial s} \bar{e}_t + \theta_t \kappa_o \bar{e}_1 + \frac{\partial}{\partial s} \theta_1 \bar{e}_1 + \theta_1 (\tau_o \bar{e}_2 - \kappa_o \bar{e}_t) + \frac{\partial \theta_2}{\partial s} \bar{e}_2 - \theta_2 \tau_o \bar{e}_1 \\ = \frac{M_t}{\beta_t} \bar{e}_t + \frac{M_1}{\beta_1} \bar{e}_1 + \frac{M_2}{\beta_2} \bar{e}_2 \end{aligned} \quad \dots \text{(A.II.3)}$$

From (A.II.2) similarly

$$\begin{aligned} \frac{\partial u_t}{\partial s} \bar{e}_t + u_t \kappa_o \bar{e}_1 + \frac{\partial u_1}{\partial s} \bar{e}_1 + u_1 (\tau_o \bar{e}_2 - \kappa_o \bar{e}_t) + \frac{\partial u_2}{\partial s} \bar{e}_2 - u_2 \tau_o \bar{e}_1 \\ = \frac{N_t}{\sigma_t} \bar{e}_t + \left(\frac{Q_1}{\sigma_1} + \theta_2\right) \bar{e}_1 + \left(\frac{Q_2}{\sigma_2} - \theta_1\right) \bar{e}_2 \end{aligned} \quad \dots \text{(A.II.4)}$$

Collecting terms from (A.II.3) and (A.II.4) and normalising the equations yields

$$aM_t = \beta_t [\theta_t' - \kappa \theta_1] \quad \dots \text{(A.II.5a)}$$

$$aM_1 = \beta_1 [\theta_t \kappa + \theta_1' - \theta_2 \tau] \quad \dots \text{(A.II.5b)}$$

$$aM_2 = \beta_2 [\theta_1 \tau + \theta_2'] \quad \dots \text{(A.II.5c)}$$

$$N_t = \sigma_t [U_t' - \kappa U_1] \quad \dots \text{(A.II.5d)}$$

$$\frac{Q_1}{\sigma_1} + \theta_2 = U_t \kappa + U_1' - U_2 \tau \quad \dots (\text{A.II.5e})$$

$$\frac{Q_2}{\sigma_2} - \theta_1 = U_1 \tau + U_2' \quad \dots (\text{A.II.5f})$$

If shear deformation is neglected, then $\sigma_1 = \sigma_2 \rightarrow \infty$.

Using the last two equations, substitute for θ_1 and θ_2 in the first three equations to yield

$$aM_t = GI_p [\theta_t' + \kappa \tau U_1 + \kappa U_2']$$

$$aM_1 = EI [\kappa \theta_t - \tau \kappa U_t - \tau' U_1 - 2\tau U_1' + \tau^2 U_2 - U_2'']$$

$$aM_2 = EI [\kappa U_t' + \kappa' U_t + U_1'' - \tau^2 U_1 - 2\tau U_2' - \tau' U_2]$$

and $N_t = EA [U_t' - \kappa U_1]$

which are the free-displacement relationships.

VI. Flow Charts and Computer Program

The flow charts shown in figures A.3 and A.4 show a brief outline of the computer programs used for the analytical results. No attempt has been made to show the details involved in the programs. However, figure A.3 shows a great deal of the Wave Propagation Program, as this was relatively simple.

Figure A.5 is the actual program used for the General Solution method. The appropriate boundary conditions must be chosen for the system under study.

FLOW CHART-WAVE PROPAGATION PROBLEM

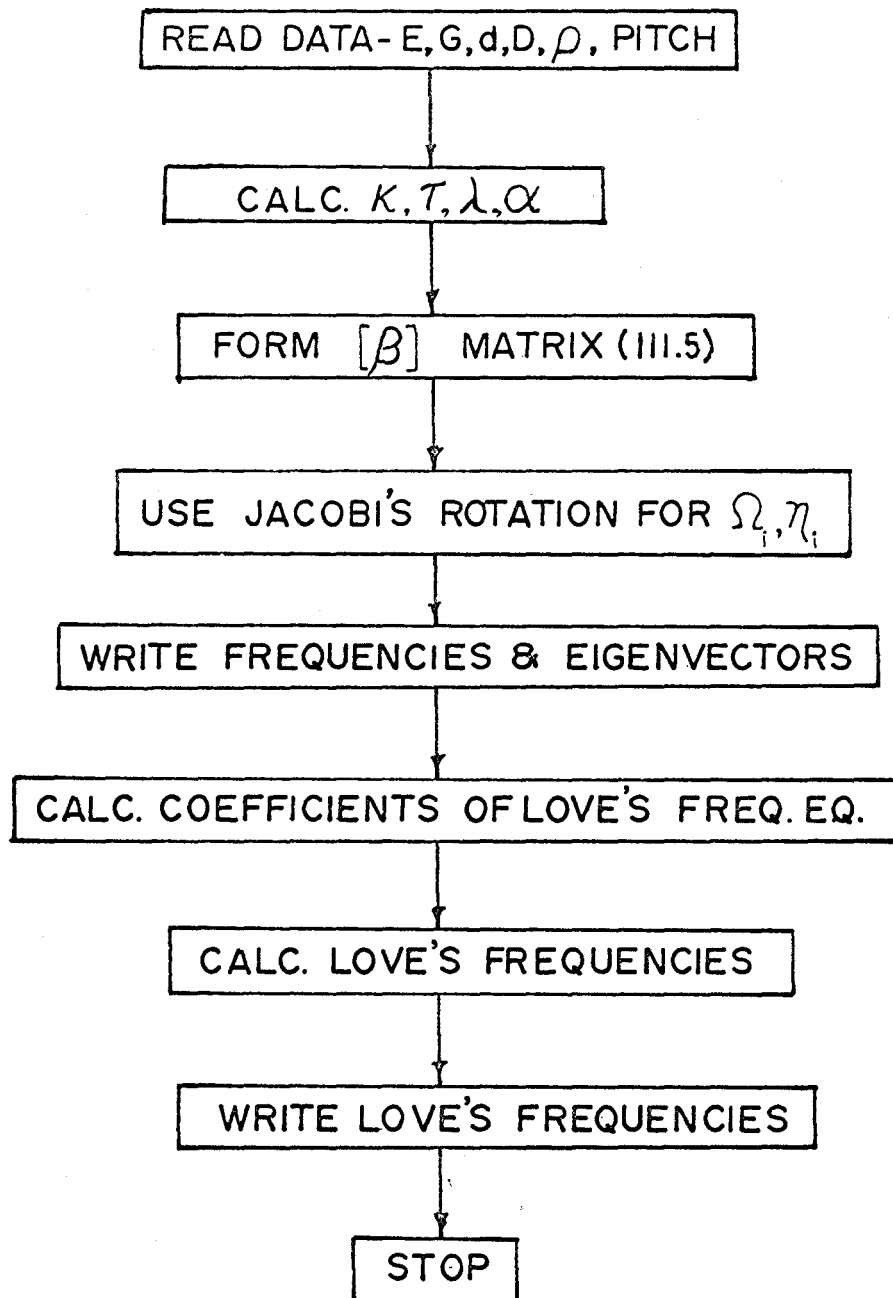
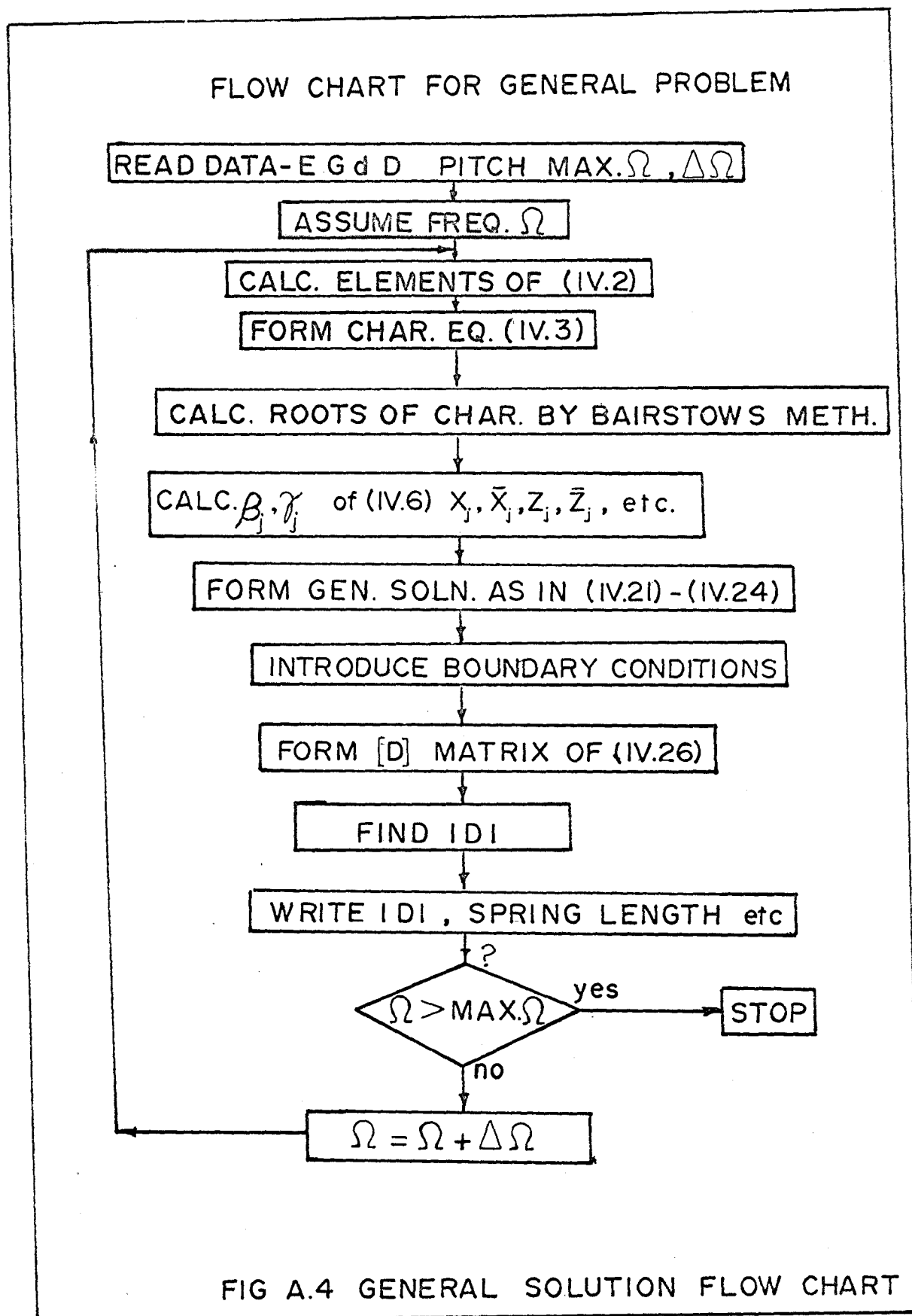


FIG A.3 WAVE PROPAGATION FLOW CHART



SJOB 003321 K PILGRIM 100 010 030
 \$IBJOB NODECK
 \$IBFTC MAINDK

DOUBLE PRECISION K,K2,K4,K6,T,T2,T4,T6,AL,C1,C2,C3,EB,FRQ2,VALDET,
 1F1,F2,F3,F4,F5,F6,V,YYY,DET,DETER,W,P,ZZ,TT,X,XX,AL
 DIMENSION EB(7),A(12),B(12),AC(13),YY(12),Y(12),REAYY(12),AIMYY(12
 1),DETER(12,12),DET(12,12)
 COMPLEX Y,A,B,YY
 LOGICAL PIMAG,COMLX,PREAL
 COMMON Y,PLNG,CONVG,OVFLOW,UNFLOW,EPS,PINFIN,K

C

C

E,G = YOUNG'S AND SHEAR MODULUS

C

RHO = DENSITY TWOPI=2.*PI

C

RODIAM=ROD DIAMETER

C

DIAM= SPRING DIAM(OUT TO OUT OF COIL)

C

PTCH=ITCH (OUT TO OUT OF COIL)

C

READ(5,92)E,G,RHO,TWOPI,RODIAM,DIAM,PTCH

92 FORMAT(3E10.0,F10.0,3F5.0)

C

TL IS THE ITERATION TOLERANCE FOR DETERMINING THE

C

RESONANCE FREQUENCY. IF THE FREQUENCY INTERVAL IN WHICH

C

WE ARE WORKING IS LESS THAN OR EQUAL TO TL, WE SAY WE HAVE

C

FOUND THE RESONANCE FREQUENCY.

READ(5,1)UNFLOW,OVFLOW,EPS,PINFIN,TL

1 FORMAT(4E6.0,F10.0)

C

IROOTS,IDIAG,IDET,IDI AEL ARE CONTROL NUMBERS.

C

IF THEY ARE NEGATIVE OR POSITIVE, CERTAIN INFORMATION IS WRITTEN

C

I.E. THE ROOTS, THE TRIANGULISED MATRIX, THE 12*12 DETERMINANT ETC.

C

IF ZERO, THESE BITS OF INFORMATION ARE NOT WRITTEN IN OUTPUT.

C

NOCARD= NO. OF DATA CARDS TO BE READ --SEE FORMAT 14.

C

READ(5,93) IROOTS,IDIAG,IDET,IDI AEL,NOCARD

93 FORMAT(5I2)

RGYR=RODIAM/4.

CONST=TWOPI**2*RHO*RGYR**2/E

CONS=360./TWOPI

COILD=DIAM-RODIAM

PITCH=PTCH-RODIAM

PIT=PITCH/TWOPI

ANGLE=ATAN(2.0*PIT/COILD)

ANG=ANGLE*CONS

K=COS(ANGLE)**2*RODIAM/(2.0*COILD)

T=K*TAN(ANGLE)

K2=K**2

K4=K2**2

T2=T**2

T4=T2**2

T6=T2*T4

K6=K2*K4

AL=2.*G/E

C1=6.*AL*(2.*K2*T2+K4+T4)

C2=4.*AL*(T6+3.*K4*T2+3.*T4*K2+K6)

C3=AL*(T2*T6+K2*K6+4.*(T6*K2+K6*T2+1.5*T4*K4))

C

AC(I)= THE COEFFICIENTS IN EQUATIONS IV.12 AND IV.13

C

C

```

AC(1)=-4.*AL*T
AC(2)=4.*AL*T2*T+K2*T*(2.-6.*AL)
AC(3)=2.*(1.-AL)*K2*T*(K2-T2)
AC(4)=-AL
AC(5)=2.*AL*(3.*T2-K2)
AC(8)=K*T*(2.+AL)
AC(9)=T*K2*K
AC(10)=K*(1.+AL)
AC(11)=-K*T2
AC(12)=AL
AC(13)=-K2
F1=4.*AL*(K2+T2)
F2=K2*(1.-3.*AL)+12.*AL*T2
F3=2.*K4+(6.*AL-6.)*T2*K2-2.*AL*T4
F4=2.*T2*K2+K4+T4
F5=K2*(AL+1.)
F6=K2*T2*2.*(AL-2.)-AL*(K4+T4)
DO 15 MIT=1,NOCARD

```

C
C
C
C

```

OMEGA=FIRST TRIAL FREQUENCY, OMEGL THE MAX., OMEGI THE INCREMENT.
TURNS= NUMBER OF TURNS IN SPRING.

```

```

READ(5,14)OMEGA,OMEGL,OMEGI,TURNS
14 FORMAT(4F5.0)
SNO=TURNS*TWOPI
WRITE(6,59)
59 FORMAT(1H1/14H          ANGLE,10X,5HPITCH,6X,13HROD DIAMETER,2X,13
1HCOIL DIAMETER,4X,9HCURVATURE,7X,7HTORSION,7X,12HNORM LENGTH)
WRITE(6,58)
58 FORMAT(13H          DEG,12X,3HIN.,12X,3HIN.,12X,3HIN.)
SLNGTH=SQRT((COILD/2.)**2+PIT**2)*SNO
PLNG=SLNGTH/RGYR
RPLNG=RGYR/SLNGTH
WRITE(6,64)ANG,PITCH,RODIAM,COILD,K,T,PLNG,RPLNG
64 FORMAT(1H0,7F15.5,E15.5)

```

C
C
C
C
C

```

FROM(110) TO (115) WE TAKE A FREQUENCY AND FIND VALUE OF
DETERMINANT D. WE NOTE THIS VALUE, INCREASE FREQUENCY BY
OMEGI AND FIND A NEW VALUE AGAIN.

```

```

110 OMI=OMEGI
ICOUNT=0
ILW=0
NM=0
D1=0.
OM=0.

```

C
C
C

```

CALCULATE SQUARE OF NORMALISED FREQUENCY

```

```

130 FRQ2=OMEGA*OMEGA*CONST
EB(1)=AL
EB(2)=F1
EB(3)=C1-2.*AL*FRQ2
EB(4)=C2+FRQ2*F2
EB(5)=C3+FRQ2*(F3+AL*FRQ2)
EB(6)=F5*FRQ2*(F4-FRQ2)

```

```

EB(7)=K4*FRQ2**2
AC(6)=F6+AL*FRQ2
AC(7)=-K2*FRQ2

```

C
C
C
C
C

```

CALL ROOTS2 TO GET ROOTS OF CHARACTERISTIC EQUATION.
IF IROOTS IS + OR - THE ROOTS ARE WRITTEN--- IF ZERO, NOTHING
IS WRITTEN.

```

```

CALL ROOTS2(EB,Y,IROOTS)
DO 117 I=1,11,2
117 YY(I)=Y(I)**2
DO 119 I=1,11,2
119 A(I)=-((Y(I)*(AC(3)+YY(I)*(AC(2)+YY(I)*AC(1))))/(AC(7)+YY(I)*(AC(6)
1+YY(I)*(AC(5)+YY(I)*AC(4))))
DO 122 I=1,11,2
122 B(I)=(AC(9)+Y(I)*(A(I)*AC(11)+Y(I)*(AC(8)+Y(I)*(A(I)*AC(10)))))/(-
1Y(I)*(AC(13)+YY(I)*AC(12)))
DO 21 J=1,11,2
REAYY(J)=REAL(Y(J))
21 AIMYY(J)=AIMAG(Y(J))

```

C
C
C
C
C

```

TESTS TO SEE WHETHER ROOT IS PURE IMAGINARY, COMPLEX OR REAL.
AFTER THIS DECISION IS MADE, TWO COLUMNS OF THE 12*12 MATRIX
ARE OBTAINED FROM THE SUBROUTINES PIMAGI,CMLXI,OR PREALI.

```

```

450 DO 700 J=1,11,2
PIMAG=REAYY(J).EQ.0.0.AND.AIMYY(J).NE.0.0
IF(PIMAG)GO TO 73
COMLX=REAYY(J).NE.0.0.AND.AIMYY(J).NE.0.0
IF(COMLX) GO TO 74
PREAL=REAYY(J).NE.0.0.AND.AIMYY(J).EQ.0.0
IF(PREAL)GO TO 71
73 X=AIMAG(A(J))
XX=AIMAG(B(J))
CALL PIMAGI(X,XX,J,DET)
GO TO 70
74 W=REAL(A(J))
P=REAL(B(J))
ZZ=AIMAG(A(J))
TT=AIMAG(B(J))
CALL CMLXI(W,P,ZZ,TT,J,DET)
GO TO 70
71 V=REAL(A(J))
YYY=REAL(B(J))
CALL PREALI(V,YYY,J,DET)
70 JJ=J+1
DO 700 L=J,JJ
DO 700 I=1,12
700 DETER(I,L)=DET(I,L)

```

C
C
C
C
C
C
C

```

WE HAVE FORMED THE 12*12 DETERMINANT. IF WE WANT TO WRITE
IT OUT THEN IDET MUST BE + OR -.IF WE DON'T WANT IT
IDET MUST BE ZERO.

```

```

      IF(IDET)540,530,540
540 WRITE(6,1214)((DETER(I,J),J=1,12),I=1,12)
1214 FORMAT(1X,12E10.3)
C
C   WE THEN CALL DETTRI, TAKING INTO THAT SUBROUTINE THE 12*12
C   DETERMINANT, IDIAG, AND IDIAEL IN ORDER TO GET THE DETERMINANT
C   OF THE 12*12 MATRIX.
530 CALL DETTRI(DETER,VALDET,FACTOR,NN,IDIAG,IDIAEL)
      WRITE(6,193)OMEGA,FRQ2,VALDET,FACTOR,NN
193 FORMAT(1H0,10HFREQUENCY=,F7.2,1X,3HCPS,5X,20HNORM. FREQ. SQUARED=,
1E18.8,5X,12HDETERMINANT=,1PE20.8,5X,7HFACTOR=,1PE11.2,1X,2H**,I2)
      IF((OMEGA-OM).LE.TL) GO TO 260
      ICOUNT=ICOUNT+1
      IF(OMEGA.GT.OMEGL) GO TO 15
      IF(ICOUNT.GT.1) GO TO 230
210 D1=VALDET
      OM=OMEGA
      IF(ILW.GE.1) OMI=0.5*OMI
      OMEGA=OMEGA+OMI
      GO TO 130
230 IF(D1*VALDET) 240,260,210
260 WRITE(6,194)
194 FORMAT(1H0,19HRESONANCE FREQUENCY)
      IF(NM.LE.1) OMEGAS=OMEGA
      OMEGA=OMEGAS
      GO TO 110
240 NM=NM+1
      ILW=ILW+1
      IF(NM.EQ.1) OMEGAS=OMEGA
      OMI=0.5*OMI
      OMEGA=OM+OMI
      GO TO 130
15 CONTINUE
250 CALL EXIT
      END
$IBFTC ROOTS2
      SUBROUTINE ROOTS2(CO,SS,IROOTS)
      COMPLEX X,Y,TEMP,P,SS
      DIMENSION CO(7),S(6),X(6),R(6),RI(6),Y(12),P(12),AIMP(12),
1REALP(12),SI(6),REAPP(12),AIMPP(12),SS(12)
      DOUBLE PRECISION CO,S,SI
      LOGICAL SHUFF1,SHUFF2,SHUFF3,PIMAG,COMP,PREAL
C
C   USE BAIRSTOW'S METHOD TO FIND ROOTS OF CHAR EQUATION
C
      CALL DBAIRS(CO,S,SI,6)
      DO 11 I=1,6
      R(I)=S(I)
11 RI(I)=SI(I)
      DO 29 I=1,6
29 X(I)=CMPLX(R(I),RI(I))
      DO 17 I=1,6
      Y(2*I-1)=CSQRT(X(I))
17 Y(2*I)=-Y(2*I-1)
      DO 52 I=1,12
      P(I)=Y(I)

```

```

REALP(I)=REAL(P(I))
52 AIMPP(I)=AIMAG(P(I))

```

C
C
C
C
C

THE COMPLEX ROOTS WILL OCCUR IN GROUPS OF 4.
THIS READJUSTS THEM IN 2 GROUPS OF 2, EACH GROUP 2 BEING
A COMPLEX PAIR-- I.E. THEY ARE CONJUGATES.

```

DO 15 I=1,9,4
SHUFF3=ABS(REALP(I)).NE.0.0.AND.ABS(AIMPP(I)).NE.0.0
IF(SHUFF3)GO TO 16
GO TO 15
16 TEMP=P(I+1)
P(I+1)=P(I+2)
P(I+2)=P(I+3)
P(I+3)=TEMP
15 CONTINUE
DO 13 I=1,11,2
SHUFF2=ABS(REALP(I)).EQ.0.0
IF(SHUFF2)GO TO 9
SHUFF1=ABS(AIMPP(I)).EQ.0.0
IF(SHUFF1)GO TO 7
GO TO 13
7 P(I)=CMPLX(REALP(I),0.)
P(I+1)=CMPLX(-REALP(I),0.)
GO TO 13
9 P(I)=CMPLX(0.,AIMPP(I))
P(I+1)=CONJG(P(I))
13 CONTINUE
IF(IROOTS) 30,31,30
30 WRITE(6,51)
51 FORMAT(10X,17HSQ. ROOT OF ROOTS,23X,14HSHUFFLED ROOTS,23X,13HORDER
IED ROOTS)
31 DO 14 I=1,11,2
REAPP(I)=REAL(P(I))
14 AIMPP(I)=AIMAG(P(I))
K=0
DO 1 I=1,11,2
PIMAG=REAPP(I).EQ.0.0.AND.AIMPP(I).NE.0.0
IF(PIMAG) GO TO 3
GO TO 1
3 K=K+1
SS(K)=P(I)
K=K+1
SS(K)=P(I+1)
1 CONTINUE
DO 4 I=1,11,2
COMP=REAPP(I).NE.0.0.AND.AIMPP(I).NE.0.0
IF(COMP) GO TO 5
GO TO 4
5 K=K+1
SS(K)=P(I)
K=K+1
SS(K)=P(I+1)
4 CONTINUE
IF(K.EQ.12) GO TO 66
DO 6 I=1,11,2

```



```

DO 104 MULT=J,12
104 A(N,MULT)=A(N,MULT)-A(J,MULT)/A(J,J)*DIV
99 CONTINUE
IF(IDIAG) 2,11,2
2 WRITE(6,1213)((A(I,J),J=1,12),I=1,12)
1213 FORMAT(1X,12E10.3)
11 IF(IDIAEL) 20,21,20
20 WRITE(6,106)
106 FORMAT(1X,58HPRODUCT OF THESE DIAGONAL ELEMENTS = DETERMINANT OF M
MATRIX)
WRITE(6,107)(A(I,I),I=1,12)
107 FORMAT(1X,6E17.8)
21 DO 3 I=1,12
3 IF(A(I,I).EQ.0.) GO TO 5
GO TO 7
5 WRITE(6,4)
4 FORMAT(1H0,34HAT LEAST ONE TERM ON DIAGONAL = 0.)
FACT=1.
VALDET=0.
L=0
GO TO 109
7 NBIG=0
NSMALL=0
VALDET=1.
DO 105 I=1,12
VALDET=VALDET*A(I,I)
IF(DABS(VALDET).LT.UNFLOW) GO TO 108
IF(DABS(VALDET).GT.OVFLOW) GO TO 110
GO TO 105
108 FACT=PINFIN
NBIG=NBIG+1
GO TO 1070
110 FACT=EPS
NSMALL=NSMALL+1
1070 VALDET=VALDET*FACT
IF(DABS(VALDET).LT.UNFLOW) GO TO 108
IF(DABS(VALDET).GT.OVFLOW) GO TO 110
105 CONTINUE
IF(NBIG-NSMALL) 14,13,15
14 L=NSMALL-NBIG
FACT=PINFIN
GO TO 109
15 L=NBIG-NSMALL
FACT=EPS
GO TO 109
13 L=0
FACT=1.
109 CONTINUE
RETURN
END

```

C THIS PACKAGE OF SUBROUTINES PIMAGI,CMLXI,AND PREALI IS FOR
 C BOUNDARY CONDITIONS AS STATED IN EQUATION(IV.25).
 C THE SUBROUTINES EVALUATE THE ELEMENTS OF TWO COLUMNS IN THE
 C D MATRIX FOR ANY ONE ROOT.

\$IBFTC PIMAGI

SUBROUTINE PIMAGI(X,XX,J,DET)

COMPLEX Y

DOUBLE PRECISION CUV,X,XX,DET,S,S2,S3,C,SZ,COSSZ,SINSZ,Z,C1
 DIMENSION DET(12,12),Y(12)

COMMON Y,PLNG,CONVG,OVFLOW,UNFLOW,EPS,PINFIN,CUV

S=AIMAG(Y(J))

S2=S*S

S3=S*S2

C=CUV/S

C1=S2*X

Z=0.

DO 30 K=1,7,6

SZ=S*Z

COSSZ=DCOS(SZ)

SINSZ=DSIN(SZ)

DET(K,J)=-C*COSSZ

DET(K,J+1)=C*SINSZ

DET(K+1,J)=S*COSSZ

DET(K+1,J+1)=-S*SINSZ

DET(K+2,J)=X*COSSZ

DET(K+2,J+1)=-X*SINSZ

DET(K+3,J)=XX*COSSZ

DET(K+3,J+1)=-XX*SINSZ

DET(K+4,J)=-C1*COSSZ

DET(K+4,J+1)=C1*SINSZ

DET(K+5,J)=-S3*COSSZ

DET(K+5,J+1)=S3*SINSZ

30 Z=PLNG

RETURN

END

\$IBFTC CMLXI

SUBROUTINE CMLXI(W,P,ZZ,T,J,DET)

COMPLEX Y

DOUBLE PRECISION CUV,W,P,ZZ,T,DET,R,S,R2,S2,R3,S3,C,SZ,Z,
 1SINSZE,COSSZE,EXX,C1,C2,C3,C4

DIMENSION DET(12,12),Y(12)

COMMON Y,PLNG,CONVG,OVFLOW,UNFLOW,EPS,PINFIN,CUV

R=REAL(Y(J))

S=AIMAG(Y(J))

R2=R*R

R3=R2*R

S2=S*S

S3=S2*S

C=CUV/(R2+S2)

C1=(R2-S2)*W-2.*R*S*ZZ

C2=(R2-S2)*ZZ+2.*R*S*W

C3=R*(R2-3.*S2)

C4=S*(3.*R2-S2)

Z=0.

DO 30 K=1,7,6

```

SZ=S*Z
EXX=DEXP(R*Z)
COSSZE=DCOS(SZ)*EXX
SINSZE=DSIN(SZ)*EXX
DET(K,J)=C*(R*SINSZE-S*COSSZE)
DET(K,J+1)=C*(R*COSSZE+S*SINSZE)
DET(K+1,J)=R*SINSZE+S*COSSZE
DET(K+1,J+1)=R*COSSZE-S*SINSZE
DET(K+2,J)=ZZ*COSSZE+W*SINSZE
DET(K+2,J+1)=W*COSSZE-ZZ*SINSZE
DET(K+3,J)=T*COSSZE+P*SINSZE
DET(K+3,J+1)=P*COSSZE-T*SINSZE
DET(K+4,J)=C1*SINSZE+C2*COSSZE
DET(K+4,J+1)=C1*COSSZE-C2*SINSZE
DET(K+5,J)=C3*SINSZE+C4*COSSZE
DET(K+5,J+1)=C3*COSSZE-C4*SINSZE
30 Z=PLNG
RETURN
END
$IBFTC PREALI
SUBROUTINE PREALI(V,YY,J,DET)
COMPLEX Y
DOUBLE PRECISION CUV,D,E,R,R2,R3,C,V,DET,YY,Z,RZ,R2V
DIMENSION DET(12,12),Y(12)
COMMON Y,PLNG,CONVG,OVFLOW,UNFLOW,EPS,PINFIN,CUV
R=REAL(Y(J))
R2=R*R
R3=R2*R
C=CUV/R
R2V=R2*V
Z=0.
DO 30 K=1,7,6
RZ=R*Z
D=DCOSH(RZ)
E=DSINH(RZ)
DET(K,J)=C*D
DET(K,J+1)=C*E
DET(K+1,J)=R*D
DET(K+1,J+1)=R*E
DET(K+2,J)=V*D
DET(K+2,J+1)=V*E
DET(K+3,J)=YY*D
DET(K+3,J+1)=YY*E
DET(K+4,J)=R2V*D
DET(K+4,J+1)=R2V*E
DET(K+5,J)=R3*D
DET(K+5,J+1)=R3*E
30 Z=PLNG
RETURN
END

```

C THIS PACKAGE OF SUBROUTINES PIMAGI,CMLXI,AND PREALI IS FOR
 C BOUNDARY CONDITIONS AS STATED IN EQUATION(V.1).
 C THE SUBROUTINES EVALUATE THE ELEMENTS OF TWO COLUMNS IN THE
 C D MATRIX FOR ANY ONE ROOT

\$IBFTC PIMAGI

```

SUBROUTINE PIMAGI(X,XX,J,DET)
COMPLEX Y
DOUBLE PRECISION CUV,X,XX,DET,S,SZ,COSSZ,SINSZ,Z,C
DIMENSION DET(12,12),Y(12)
COMMON Y,PLNG,CONVG,OVFLOW,UNFLOW,EPS,PINFIN,CUV
S=AIMAG(Y(J))
Z=0.
C=CUV/S
DO 30 K=1,7,6
SZ=S*Z
COSSZ=DCOS(SZ)
SINSZ=DSIN(SZ)
DET(K,J)=-C*COSSZ
DET(K,J+1)=C*SINSZ
DET(K+1,J)=SINSZ
DET(K+1,J+1)=COSSZ
DET(K+2,J)=S*COSSZ
DET(K+2,J+1)=-S*SINSZ
DET(K+3,J)=X*COSSZ
DET(K+3,J+1)=-X*SINSZ
DET(K+4,J)=-X*S*SINSZ
DET(K+4,J+1)=-X*S*COSSZ
DET(K+5,J)=XX*COSSZ
DET(K+5,J+1)=-XX*SINSZ
30 Z=PLNG
RETURN
END

```

\$IBFTC CMLXI

```

SUBROUTINE CMLXI(W,P,ZZ,T,J,DET)
COMPLEX Y
DOUBLE PRECISION CUV,W,P,ZZ,T,DET,R,S,SZ,Z,SINSZE,COSSZE,EXX,
1C1,C2,C
DIMENSION DET(12,12),Y(12)
COMMON Y,PLNG,CONVG,OVFLOW,UNFLOW,EPS,PINFIN,CUV
R=REAL(Y(J))
S=AIMAG(Y(J))
C1=R*ZZ+W*S
C2=R*W-ZZ*S
C=CUV/(R**2+S**2)
Z=0.
DO 30 K=1,7,6
SZ=S*Z
EXX=DEXP(R*Z)
COSSZE=DCOS(SZ)*EXX
SINSZE=DSIN(SZ)*EXX
DET(K,J)=C*(R*SINSZE-S*COSSZE)
DET(K,J+1)=C*(R*COSSZE+S*SINSZE)
DET(K+1,J)=SINSZE
DET(K+1,J+1)=COSSZE
DET(K+2,J)=R*SINSZE+S*COSSZE

```

```

DET(K+2,J+1)=R*COSSZE-S*SINSZE
DET(K+3,J)=ZZ*COSSZE+W*SINSZE
DET(K+3,J+1)=W*COSSZE-ZZ*SINSZE
DET(K+4,J)=C1*COSSZE+C2*SINSZE
DET(K+4,J+1)=C2*COSSZE-C1*SINSZE
DET(K+5,J)=T*COSSZE+P*SINSZE
DET(K+5,J+1)=P*COSSZE-T*SINSZE
30 Z=PLNG
RETURN
END
$IBFTC PREALI
SUBROUTINE PREALI(V,YY,J,DET)
COMPLEX Y
DOUBLE PRECISION CUV,D,E,R,V,DET,YY,Z,RZ,C
COMMON Y,PLNG,CONVG,OVFLOW,UNFLOW,EPS,PINFIN,CUV
DIMENSION DET(12,12),Y(12)
R=REAL(Y(J))
C=CUV/R
Z=0.
DO 30 K=1,7,6
RZ=R*Z
D=DCOSH(RZ)
E=DSINH(RZ)
DET(K,J)=C*D
DET(K,J+1)=C*E
DET(K+1,J)=E
DET(K+1,J+1)=D
DET(K+2,J)=R*D
DET(K+2,J+1)=R*E
DET(K+3,J)=V*D
DET(K+3,J+1)=V*E
DET(K+4,J)=V*R*E
DET(K+4,J+1)=V*R*D
DET(K+5,J)=YY*D
DET(K+5,J+1)=YY*E
30 Z=PLNG
RETURN
END

```